ADVANCED FUNCTIONAL MATERIALS
www.afm-journal.de

Advances in Stimuli-Responsive Organic Materials and Polymers toward Intelligent CO_2 Capture

*Jian Zhou, Marc Deissenroth-Uhrig, and Markus Gallei**

Recent advances in carbon dioxide (CO_2) capture highlight the potential of stimuli-responsive organic materials and polymers as low-energy, tunable solutions for climate change. This review summarizes developments in covalent organic frameworks (COFs), metal organic frameworks (MOFs), porous organic polymers (POPs), and related organic materials that respond to external stimuli such as temperature, light, pH, redox, magnetism, and pressure for CO_2 capture. These materials enable controllable CO_2 adsorption and desorption, offering improved efficiency, selectivity, and recyclability. By outlining key mechanisms and feasibility of multi-stimulations, this review aims to support the rational design of scalable, energy-efficient stimuli-responsive materials for fundamental and industrial research of CO_2 capture.

1. Introduction

1.1. Significance for Carbon Neutrality

Global temperatures have been steadily rising for the past decades.[1] According to the World Meteorological Organization (WMO), 2024 has been recorded as the hottest year on record (**Figure 1A**).[2] The frequency of extreme weather is also increasing. As one of the most impactful and pervasive greenhouse gases, carbon dioxide (CO_2) has seen its atmospheric concentration increase by 21.9% over the past four decades (Figure 1B).[3] The global warming, along with the challenges of CO_2 emissions and CO_2 absorption, has become the elephant in the room — a globally critical issue that can no longer be ignored.

In order to mitigate these negative impacts, scientists and policymakers are increasingly focusing on achieving carbon neutrality goals by reducing CO_2 emissions and removing existing emissions.[5] In the carbon neutrality strategy illustrated in Figure 1C, CO_2 emission reduction and CO_2 removal represent two central components, achieved through carbon capture and storage (CCS) and negative emission technologies (NETs), respectively.[4] CO_2 emissions can be broadly categorized based on their spatial distribution into two types: centralized sources, primarily from industrial activities such as factories and power plants, which account for the majority of emissions; and decentralized sources, including transportation (e.g., cars, trains, ships) and residential energy use (e.g., natural gas, firewood). At present, most industrial CO_2 emissions from centralized sources can be addressed using CCS, whereas emissions from decentralized sources are mainly released directly into the atmosphere. CCS is widely recognized as a key approach for mitigating industrial emissions and typically involves three stages: capture, transport, and storage. In contrast, NETs focus on removing CO_2 directly from the atmosphere. When integrated with the transport and storage phases of CCS, NETs contribute to the goal of carbon neutrality. According to the latest report by the Intergovernmental Panel on Climate Change (IPCC),[6] achieving climate goals (such as limiting warming to 1.5 or 2.0 °C) requires significant reductions in greenhouse gas emissions, supplemented by various forms of NETs. NETs are not a substitute for emissions reductions but a necessary complement to achieving net zero emissions, especially for emission sources that are difficult to eliminate.

CCS and NETs are seen as an important means to bridge the "carbon balance" between human emissions and natural absorption, thereby avoiding catastrophic impacts on the ecosystem.[7] Among these technologies, CO_2 capture is the primary goal and the key parts for addressing carbon neutrality.[8] By capturing CO_2 from the air or emission sources and storing or reusing it, the process of global warming can be slowed down.[9]

1.2. Methods for CO_2 Capture

CCS is an advanced climate mitigation technology that involves the separation of CO_2 from industrial or energy-related

J. Zhou, M. Gallei
Polymer Chemistry
Saarland University
Campus C4 2, 66123 Saarbrücken, Germany
E-mail: markus.gallei@uni-saarland.de
J. Zhou, M. Gallei
Saarene
Saarland Center for Energy Materials and Sustainability
Campus C4 2, 66123 Saarbrücken, Germany
M. Deissenroth-Uhrig
School of Engineering
University of Applied Sciences (htw saar)
Goebenstraße 40, 66117 Saarbrücken, Germany

The ORCID identification number(s) for the author(s) of this article can be found under https://doi.org/10.1002/adfm.202520959

DOI: 10.1002/adfm.202520959

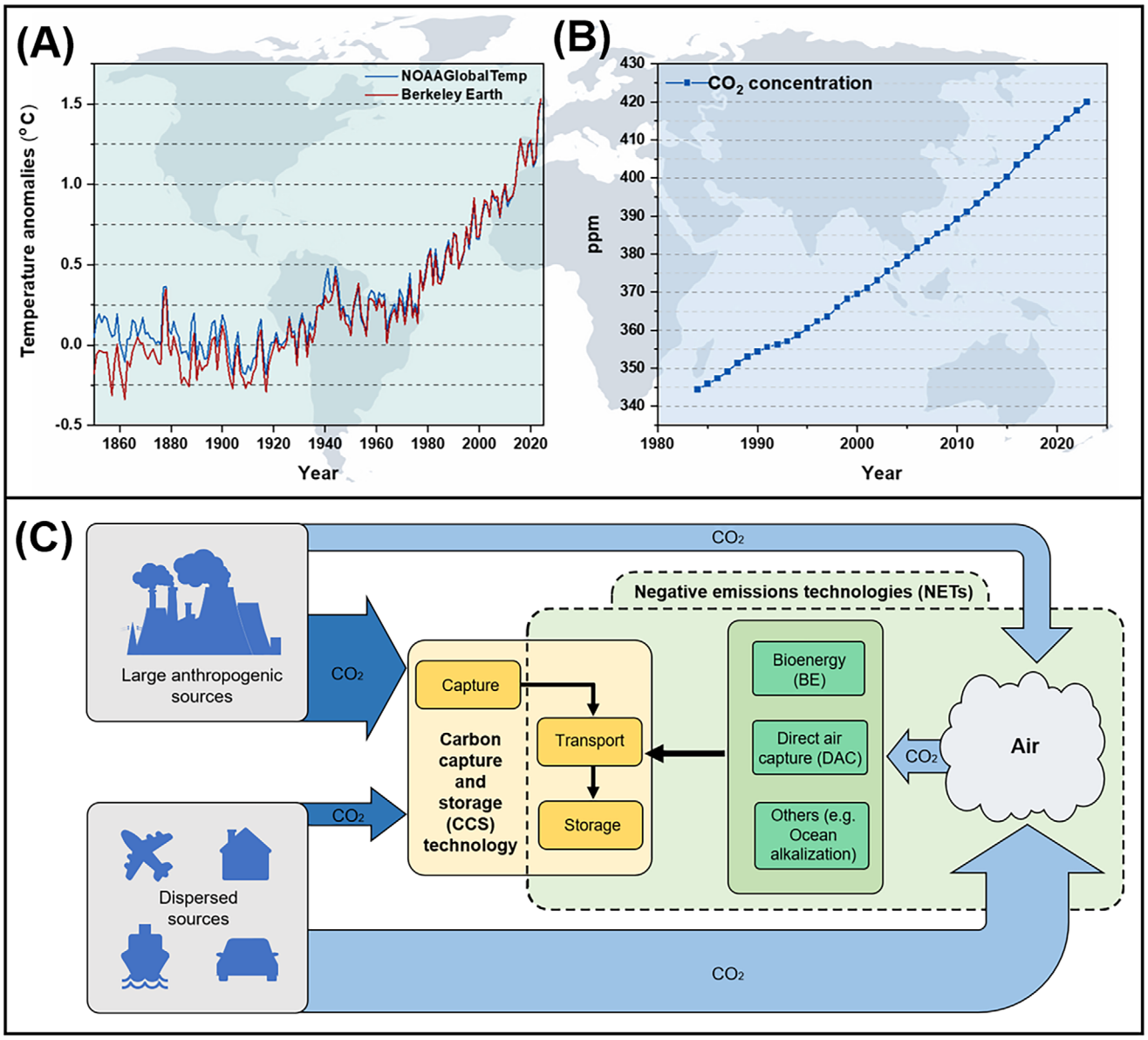

Figure 1. A) Global mean temperature from 1850 to 2024,[2] B) Atmospheric CO_2 concentration from 1984 to 2023,[3] C) Schematic diagram of relationship between carbon capture and storage (CCS) technologies and negative emissions technologies (NETs).[4]

sources, its compression and transport, and its long-term geological storage to prevent its release into the atmosphere.[10] In addition, main parts of NETs need to be integrated with CCS to enable effective CO_2 management.[11] There are three types: pre-combustion, post-combustion, and oxygen-enriched combustion.[12] Pre-combustion treatment first converts the fuel into synthesis gas (mainly CO and H_2) through gasification or reforming. Then the gas is transformed into CO_2 and H_2 via a shift reaction, after which the CO_2 is separated, leaving H_2 as the combustible fuel (**Figure** 2A). This method has advantages such as handling high CO_2 concentrations and pressures, as well as easier separation processes.[13] It can be coupled with clean energy to improve system efficiency, such as H_2. It is suitable for large-scale power generation or industrial hydrogen production projects based on coal and natural gas gasification. As contrast, post-combustion treatment directly captures CO_2 from the flue gas released from combustion by using amine absorbents (such as Monoethanolamine (MEA)) or carbonates and other methods for absorption and regeneration (Figure 2B).[14] This method can be directly applied to existing traditional power plants. In addition, the technology is mature and there are many engineering cases. It is suitable for large carbon-emitting sources, such as old thermal power plants, cement plants, and steel plants.[15] Oxygen-enriched combustion uses high-purity oxygen instead of air for combustion, so that the flue gas is mainly CO_2 and water vapor. High-purity CO_2 can be obtained after condensing the water (Figure 2C). This method has a high concentration of CO_2 after capture, which is convenient for compression and

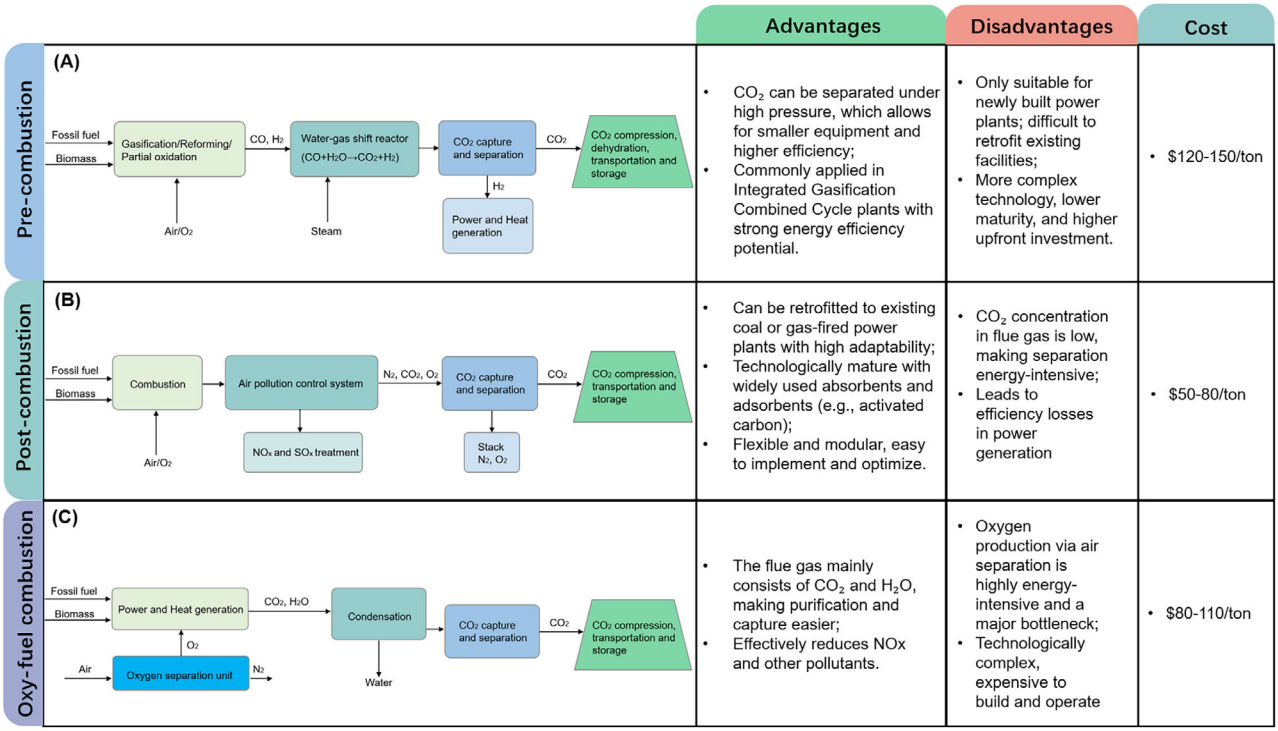

Figure 2. A) Pre-combustion CO_2 capture technology, B) post-combustion CO_2 capture technology, C) oxy-fuel CO_2 capture technology, and their advantages,[17] disadvantages,[9,18] costs of each technology.[19]

transportation. It can also simplify the separation process and save solvent use.[16]

Pre-combustion capture separates CO_2 before fuel combustion, offering higher thermal efficiency but requiring complex processes and significant infrastructure investment.[20] Oxy-fuel combustion utilizes pure oxygen to reduce flue gas volume and increase CO_2 concentration; however, it is highly energy-intensive and economically challenging.[21] In contrast, post-combustion capture is the most widely studied and applied method due to its compatibility, making it more feasible for near-term deployment. However, its capture efficiency and selectivity may be affected by other components in the flue gas, and the solvent regeneration process also consumes a lot of energy.[22] In addition, CCS technology primarily addresses concentrated, high-concentration CO_2 emissions. However, based on strategy of negative emissions, there are numerous dispersed emissions and historical cumulative emissions of CO_2 in the air that also require treatment (Figure 1C). These applications encounter diverse environmental conditions, including varying temperatures, humidity levels, and gas concentrations. Moreover, traditional processes show that extracting 400 ppm of CO_2 from the air demands more energy than extracting 120,000 ppm from flue gas.[4] Hence, there is a pressing need to develop CO_2 capture technologies that are more efficient, cost-effective, and advanced.

1.3. Stimuli-Responsive Materials

To overcome the limitations of traditional CCS technology, researchers are actively exploring new materials for CO_2 capture. Among these, intelligent stimuli-responsive materials have garnered significant attention due to their ability to adjust their physical and chemical properties according to environmental changes, such as temperature, pH, light, redox, pressure or magnetism.[23]

Stimuli-responsive materials can be broadly divided into several categories based on their chemical composition and structural characteristics. Polymer-based responsive materials have been the most extensively studied, with representative materials including poly(*N*-isopropylacrylamide) (PNIPAAm), which exhibits significant reversible volume transitions with temperature and is widely used in drug delivery and sensing systems.[24] Coordination polymers and metal-organic frameworks (MOFs) are known for their structural tunability and multifunctionality and have shown great potential in gas sensing and energy storage applications.[25] Peptide- and protein- based materials can undergo structural transformations in response to pH or enzymatic stimuli and are well-suited for tissue engineering and biosensing.[26] Engineered living materials that integrate synthetic materials with living cells have emerged, enabling precise responses to complex biological stimuli and showing promise in environmental monitoring and drug release,[27] for example, a system of light-controllable living biomaterials by integrating engineered *E. coli* into hydrogels enabling precise spatiotemporal control of protein expression and cell behavior.[28] 2D materials such as MXenes and black phosphorus possess rapid response capabilities due to their layered structures and high surface area, which can make them suitable for flexible electronics and smart sensors.[29] Collectively, these material types exhibit distinct properties, such as temperature-responsiveness,

structural adaptability, biocompatibility, high specific surface area, and programmable bioactivity, and play critical roles in the development of intelligent systems.[30]

Stimuli-responsive organic materials and polymers have emerged as promising candidates for CO_2 capture. Compared with traditional CO_2 capture technology, these materials have the following potential advantages: higher capture efficiency and selectivity,[31] lower energy consumption[32] and more flexible applications.[33] Covalent organic frameworks (COFs), as a key example, possess well-defined porous sites and adjustable surface functionalities, enabling high CO_2 selectivity and uptake performance under both low- and high-pressure conditions.[34] Compared to "classical" stimuli such as temperature or pH, CO_2 can act as a "green trigger" for reversible polymer responses, particularly in materials functionalized with amidines, tertiary amines, or guanidines, which can make them suitable for repeated adsorption–desorption cycles without chemical contamination.[35] In addition, porous organic polymers (POPs) and ionic organic frameworks have shown excellent adsorption capacity and cyclic durability, maintaining their performance during multiple switching operations such as light-induced azobenzene isomerization.[36] The presence of ionic sites within these frameworks further enhances CO_2 affinity, and tunable counterions provide a powerful route for optimizing performance.[37] Most notably, recent advances in COF-based membrane design have demonstrated industrial potential by combining high selectivity with scalability for gas separation applications.[38] In general, these properties position materials as leading candidates in the development of low-energy, high-efficiency carbon capture systems aligned with global net-zero emission goals. Over the past decade, the concept of using CO_2 as a green and reversible trigger in polymer systems has garnered significant attention,[39] along with providing a foundation for understanding CO_2-responsive material systems and their diverse applications. Under the current climate of carbon emission control, we still need a systematic understanding of smart stimulus-responsive materials for CO_2 capture in various treatment scenarios. This review introduces the application of stimuli-responsive organic materials and polymers in carbon capture in recent years. These materials include POPs, COFs, MOFs, and some organic molecules. The stimuli include changes in pressure, temperature, light, redox, pH, and magnetism (**Figure 3**). In addition, different complex stimuli (dual- and triple-responsive) are also introduced for their promising potential applications.

2. Classification and Mechanisms of Stimuli-Responsive Organic Materials and Polymers for CO_2 Capture

2.1. Single-Responsive Materials

A wide range of external stimuli can trigger a single stimuli-responsive behavior, including temperature,[48] light,[49] magnetism,[50] pH,[51] force,[52] ultrasound,[53] redox,[54] enzymes,[55] antibodies[56] and specific biomolecules.[57] In this review, we focus on six kind of the most commonly employed stimuli in current research.

2.1.1. Light-Responsive Materials

Light- or photo-responsive materials have attracted increasing attention in CO_2 capture due to their high sensitivity and the abundance of light as an energy source.[58] These materials typically function by incorporating light-responsive moieties into their frameworks to regulate their adsorption properties. These moieties can exist as guest molecules, surface-grafted groups, or integral parts of the backbone linkers, with their photoisomerization triggering structural or electrostatic changes that enable controllable CO_2 adsorption and release.[59]

In 2013, Lyndon et al.[59] reported a metal-organic framework (MOF) material, $Zn(AzDC)(4,4'\text{-BPE})_{0.5}$, containing light-responsive moieties (**Figure 4A**). By introducing azobenzene-derived ligands, they induced a configurational change under UV irradiation, achieving a CO_2 desorption efficiency of up to 64%. Based on this theory, they[40] further developed the diversity of light-responsive materials in 2015 by incorporating photoisomerizable diarylethene (DArE) as guest molecules into the highly porous aromatic framework-1 (PAF-1) to develop DArE@PAF-1, a photodynamic CO_2 capture material (Figure 4B). Upon light irradiation, aromatic stacking and hydrogen bonding induced DArE to isomerize into an interlocked conformation, weakening CO_2-framework interactions and enabling instantaneous CO_2 release. The degree of light-response was tunable based on DArE loading, achieving up to 26 wt% CO_2 desorption. This study introduces the light response mechanism into non-metallic porous framework materials, providing a new solution to overcome the limitations of poor thermal stability and high cost of MOF.

Subsequently, Li et al.[60] introduced a non-conventional mechanism by embedding silver nanocrystals (AgNCs) into a UiO-66 framework. Under visible light irradiation, AgNCs act as "nanoheaters," converting light into localized heat and triggering the release of CO_2. This light-induced localized heating strategy achieved up to 90.5% desorption efficiency in Ag/UiO-66 composites, with fast response and good cycling stability. After verifying the feasibility of visible light regulation, the researchers shifted from material structure response to site electronic regulation mechanism. For enhancing adsorbent–adsorbate interactions, Wu et al.[61] developed light-responsive mesoporous silica functionalized with primary amines and push-pull azobenzene (Dispersed Red 1, DR1), which is responsive to visible light. Upon irradiation, DR1 underwent trans–cis isomerization, modulating the electrostatic potential of amine groups and reversibly altering CO_2 uptake. Even with strong adsorption sites, CO_2 uptake changed by up to 40%. Afterward, in the context of sustainable development, the greenness and cost of materials are increasingly valued. Liu et al.[62] utilized hypercrosslinked polymers (HCPs) derived from waste polystyrene and loaded with 8.9 wt% azobenzene. Under UV- and visible light switching, the CO_2 adsorption capacity increased by 48%, with 14% desorption achievable by visible light alone. The performance remained stable over 5 cycles, and the total regeneration cost was only 1/500 that of conventional thermal or vacuum swing methods. On this basis, the latest research in 2024 further advances light-responsive CO_2 capture to continuous flow system and water phase operation. Seo et al.[63] presented a water-based photochemical CO_2 capture and release system utilizing the photoacid pyranine (HPTS) in a bicarbonate buffer. Under visible light, the excited-state

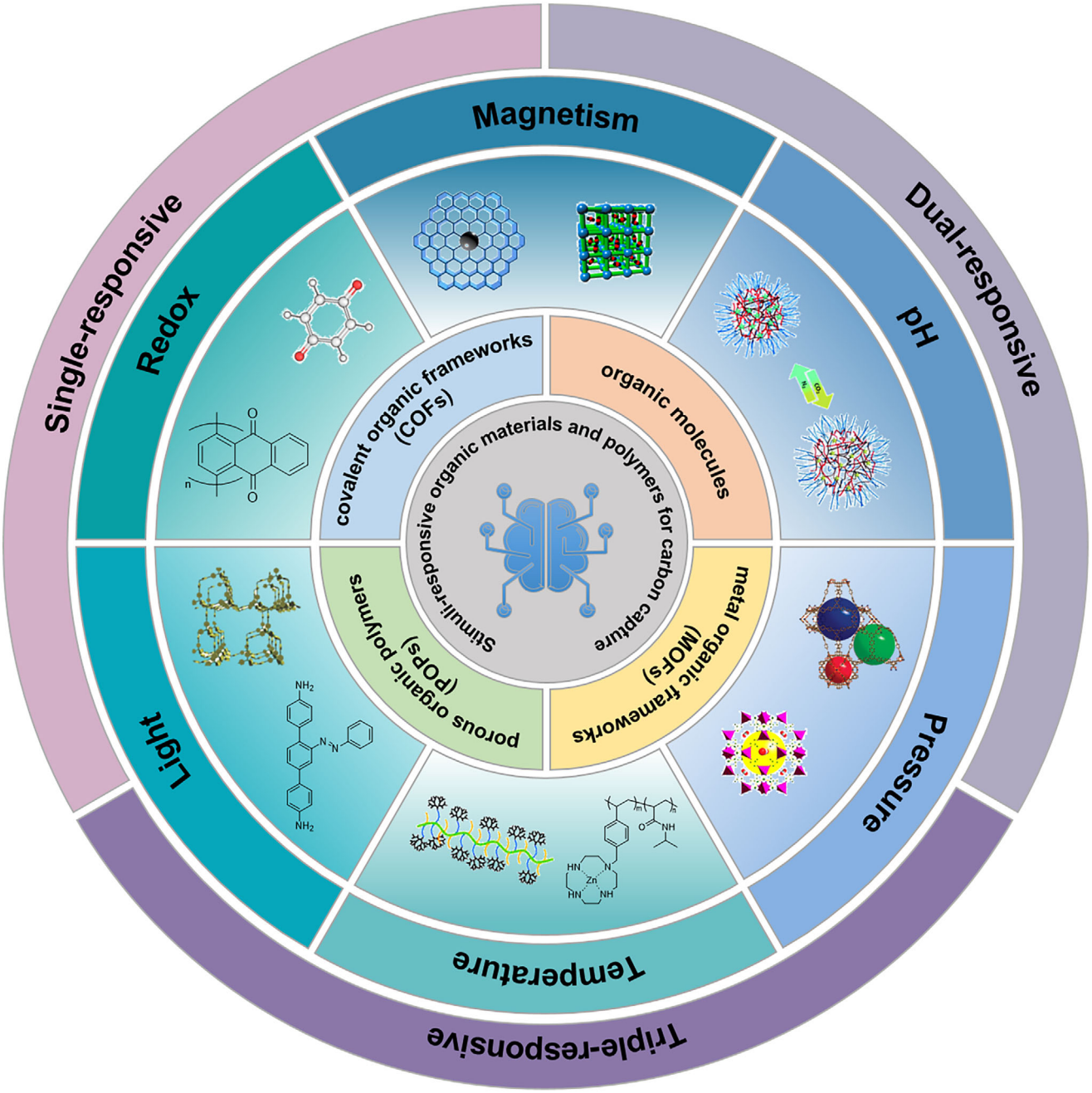

Figure 3. Schematic classification of stimuli-responsive organic materials and polymers for carbon capture applications. Light) Reproduced with permission.[40] Copyright 2015, Wiley-VCH. Redox) Adapted with permission.[41] Copyright 2022, American Chemical Society. Magnetism) Reproduced with permission.[42] Copyright 2016, Wiley-VCH. Adapted with permission.[43] Copyright 2020, Elsevier. pH) Adapted with permission.[44] Copyright 2016, RSC Publishing. Pressure) Adapted with permission.[45] Copyright 2013, American Chemical Society. Adapted with permission.[46] Copyright 2011, American Chemical Society. Temperature) Adapted with permission.[47] Copyright 2021, Elsevier.

photoacidity of HPTS decreased the pH, converting bicarbonate to carbonic acid and facilitating the release of CO_2. This system operated continuously for 7 days, capturing 60 mmol of CO_2, and demonstrated the feasibility of direct air capture under ambient conditions.

Integrating light-responsive components into adsorbent materials via various strategies enables diverse mechanisms for light-controlled CO_2 adsorption and release. However, the CO_2 release ratios of most light-responsive systems remain limited (e.g., DArE@PAF-1 exhibits a release rate of ≈26 wt%), and some materials show a significant decline in response efficiency after multiple cycles. Additionally, these materials often exhibit slow light-responsive rates and poor light penetration. Moreover, structural design issues arise due to the interference between the

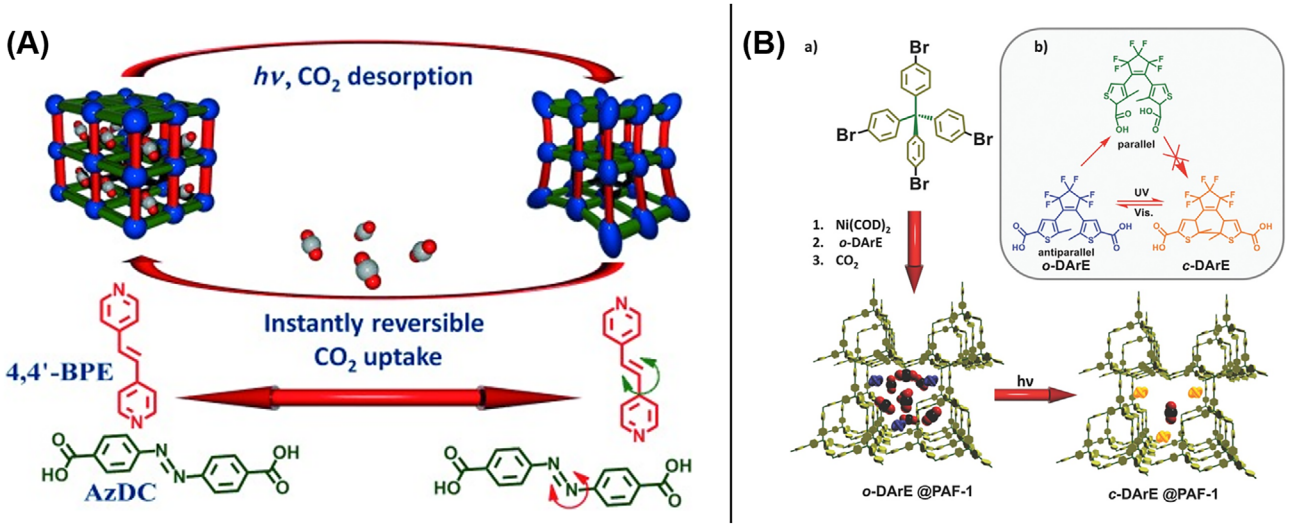

Figure 4. A) Dynamic photo-switching in the light-responsive MOF Zn(AzDC)(4,4′-BPE)0.5 leads to instantly reversible CO_2 uptake. Reproduced with permission.[59] Copyright 2013, Wiley-VCH. B) Dynamic photo-switching of light-responsive DArE@PAF-1. Broadband light irradiation of the material resulted in a spontaneous CO_2 release. a) PAF-1 is produced by a self-condensation of tetraphenylbromomethane (top left), which is then loaded with the diarylethene dye o-DArE (bottom left), which induces the release of adsorbed CO_2 upon exposure to visible light (bottom right). b) The dye undergoes a reversible cyclization reaction, which activates the PAF pores. Reproduced with permission.[40] Copyright 2015, Wiley-VCH.

light-responsive units and the porous framework, making it difficult to balance adsorption capacity and response efficiency.

2.1.2. Temperature-Responsive Materials

Temperature-responsive (thermo-responsive) materials exhibit structural deformation in response to temperature fluctuations, enabling tunable CO_2 adsorption behavior.[64] These materials often change their pore topology or undergo phase transitions, allowing dynamic control over gas separation processes. In carbon capture applications, this property enables reversible CO_2 adsorption at low temperatures and desorption at elevated temperatures, significantly reducing energy consumption and enhancing recyclability. Yue et al.[65] have designed a temperature-responsive polymer that can effectively adsorb CO_2 at lower temperatures and rapidly release CO_2 at slightly higher temperatures, thereby achieving low-energy cyclic capture. This design strategically utilizes temperature-induced changes in hydrophilicity and hydrophobicity to regulate CO_2 affinity. Hu et al.[66] developed a temperature-responsive polymer, PNiPAm-*co*-CyclenZn, which combines poly(*N*-isopropylacrylamide) (PNiPAm) with a cyclen-based zinc complex to mimic the catalytic activity of carbonic anhydrase. This polymer has a lower critical solution temperature (LCST) of 33.7 °C, below which it is in a swollen, hydrated state with enhanced catalytic activity, and above which it dehydrates and shrinks, facilitating separation from the CO_2-loaded solution. The material effectively catalyzes the reaction between CO_2 and water to form bicarbonate, with catalytic rate constants increasing at higher pH. This reversible thermal behavior aids in the efficient recovery and reuse of the catalyst during absorption-desorption cycles.

In addition to synthetic polymers, temperature-responsive strategies have also been applied to biomass-derived materials, offering environmentally friendly alternatives for efficient CO_2 capture. Liu et al.[47] developed a biomass-based temperature-responsive solid amine adsorbent, using renewable sisal fiber (SF) as the support (**Figure 5A**). The fiber surface was co-grafted with thermo-responsive *N*-isopropylacrylamide (NIPAM) and acrylamide (AM), followed by further amination with hyperbranched polyamine (HBP-NH_2) to increase the density of active amine groups. The material exhibited a distinct temperature-responsive behavior ≈50–60 °C, with a significant decrease in swelling ratio and water uptake as the temperature increased, indicating the typical hydrophilic-to-hydrophobic transition of PNIPAM (Figure 5B). By optimizing the AM/NIPAM feed ratio (1:1 being optimal), the SF-AM-co-NIPAM-HBP-NH_2 retained a high CO_2 adsorption capacity (2.61 mmol g^{-1}) while reducing the regeneration temperature to just 60 °C (Figure 5C). This represents a notable improvement over traditional solid amine adsorbents, which typically require regeneration temperatures of ≈140 °C. Moreover, the material showed excellent cycling stability over multiple adsorption-desorption cycles. However, the temperature-responsive process suffers from issues such as delayed reaction, uncontrollable foam generation, and interference from water vapor, all of which affect cycle stability and continuous operation performance. Some microgel systems experience severe foaming during CO_2 introduction, which requires a high cross-linking strategy to mitigate, however this comes at the cost of reduced material responsiveness and hydrophilicity.

2.1.3. pH-Responsive Materials

The basic principle of using pH-responsive materials for CO_2 capture is to exploit the changes in their chemical properties under different pH conditions to achieve controllable adsorption and release of CO_2.[67] These materials typically capture CO_2

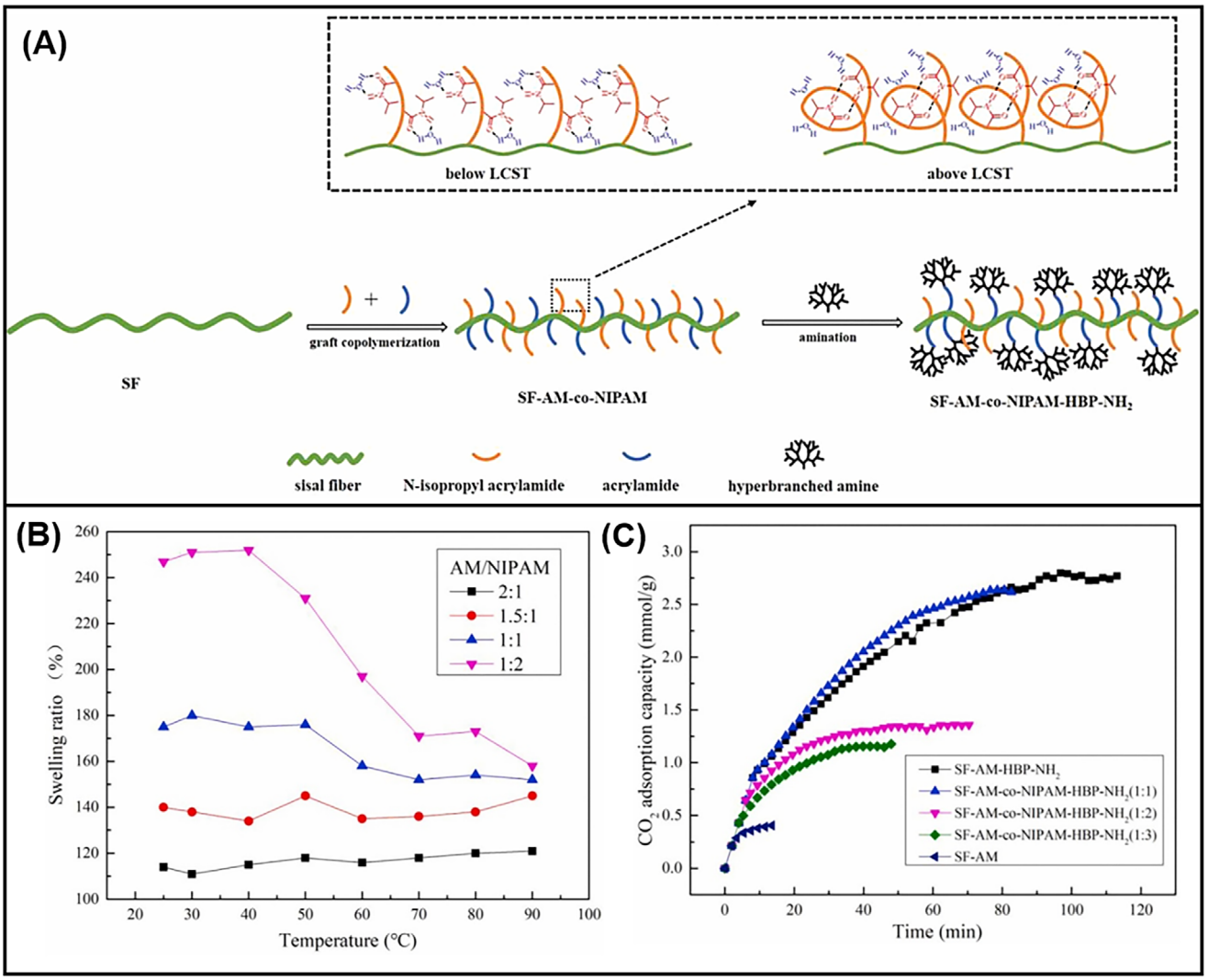

Figure 5. A) Preparation scheme and the thermo-sensitivity behavior of SF-AM-*co*-NIPAM fibers. B) Swelling ratio curve of SF-AM-*co*-NIPAM prepared with different AM/NIPAM feeding molar ratio. C) Cumulative Curves of CO_2 adsorption on the fresh grafted fibers. Adapted with permission.[47] Copyright 2021, Elsevier.

under alkaline conditions (high pH) and release it under acidic conditions (low pH), offering good reversibility and energy-saving potential.[68]

Hu et al.[69] proposed a pH-responsive phase transition mechanism. Amorphous UiO-66-SO_3H is neutralized in an alkaline solution (high pH value) to transform into crystalline UiO-66-SO_3M (M = Li, Na, K). The alkali metal ions react with –SO_3H, breaking strong hydrogen bonds and introducing –SO_3M groups, which generate electrostatic repulsion and cause the collapsed framework to unfold and restore its long-range structure. This transformation significantly increases the material's specific surface area and thermal stability, while enhancing CO_2 adsorption and CO_2/N_2 selectivity. In addition, there is another pH-responsive method that can be used for CO_2 capture. Mabireu et al.[44] developed polymeric micrometer-scale particles that exhibit CO_2/pH dual-responsiveness and incorporate built-in fluorescence as a real-time signal. The core-forming monomer, *N,N*-diethylaminoethyl methacrylate (**Figure 6**), contains tertiary amines that are protonated under acidic conditions. When CO_2 is bubbled into the aqueous medium, the pH drops due to the formation of carbonic acid, triggering protonation of the amine groups. The local polarity inside the particle core is altered, quenching the fluorescence of the embedded ABM dye (a polarity-sensitive fluorophore) and decreasing the emission intensity from 810 to 50 a.u. at 487 nm. When CO_2 is removed by N_2 bubbling, the pH increases as carbonic acids are neutralized. Tertiary amines become deprotonated, restoring the core's hydrophobicity and causing the particles to shrink. Fluorescence recovers, completing the pH-triggered reversible cycle. Although this method does not directly control the amount of CO_2 absorption by changes in pH, this method of monitoring the amount of CO_2 absorption through fluorescence changes caused by pH changes has also opened a new gate for the application of pH-responsive organic materials.

Although these systems offer advantages such as mild operating conditions and high functional integration, they still face

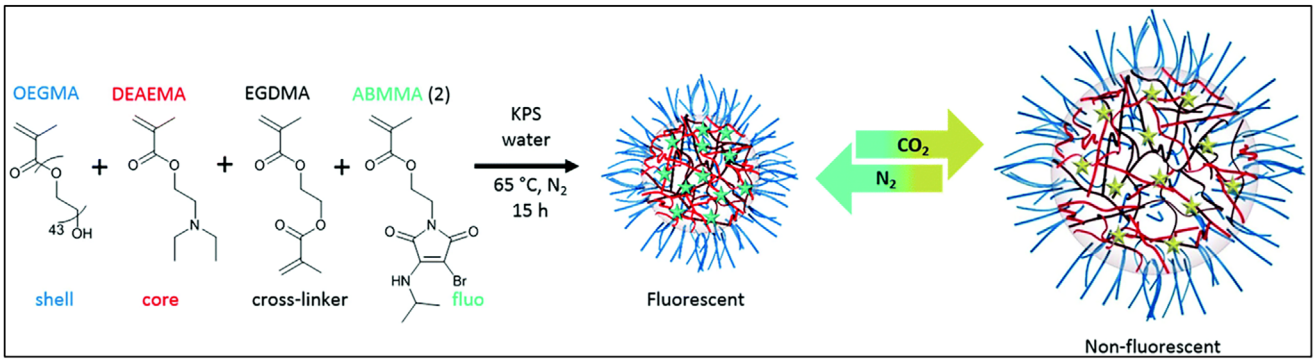

Figure 6. Synthesis of particles via emulsion polymerization in water at 65 °C and the reversible particle response upon CO_2 and N_2 bubbling. Adapted with permission.[44] Copyright 2016, RSC Publishing.

challenges including irreversible structural changes and limited response precision. For example, materials with low shell density tend to aggregate during repeated cycles, leading to irreversible changes in particle size and response behavior. In addition, the pH change induced by CO_2 is relatively slow, with the response rate constrained by dissolution and diffusion processes, making it difficult to meet the demands of rapid adsorption and release.

2.1.4. Magnetic-Responsive Materials

Magnetic-responsive materials have emerged as innovative solutions for applications such as drug delivery,[70] water purification,[71] and particularly for energy-efficient gas capture and release.[72] These materials integrate magnetic nanoparticles that respond to external magnetic fields, converting electromagnetic energy into heat, which can drive structural or sorption changes. In magnetic induction swing adsorption, magnetic nanoparticles act as nanoheaters, generating localized heat in magnetic field.[73] This enables rapid, remote regeneration of CO_2-loaded adsorbents.

In 2016, Sadiq et al.[42] evaluated the performance of magnetic-induced temperature swing adsorption (MISA) (**Figure 7A**). Building on the earlier concepts of triggering MOF regeneration using external stimuli such as light and magnetic, they uniformly embedded highly heat-efficient $MgFe_2O_4$ nanoparticles within a thermally stable and moisture-resistant Zr-based MOF (UiO-66) to create magnetic framework composites (MFCs) (Figure 7B). They achieved remote and rapid CO_2 desorption under an alternating magnetic field. With a moderate concentration of $MgFe_2O_4$ dispersed in the MOF precursor solution, CO_2 desorption exceeded 82% at a magnetic field strength (μoH) of 21 mT, and even reached 100% CO_2 desorption at 42 mT (Figure 7C). This study revealed that magnetic nanoparticles can significantly improve MOF regeneration efficiency, overcoming the slow heat transfer caused by its low thermal conductivity and achieving 100% desorption efficiency at high field strengths. However, due to the low CO_2 working capacity of the selected UiO-66 (up to 1.8 wt%), the overall regeneration energy consumption remains higher than that of some high-capacity MOF or amine solution systems. To overcome this issue, the same group[43] further optimized the material in 2020 (Figure 7D), selecting Mg-MOF-74, which has high CO_2 capacity and selectivity, and combining it with $MgFe_2O_4$ nanoparticles (Figure 7E). The hydrophobic polymer poly(1-(trimethylsilyl)-1-propyne) (PTMSP) was also introduced to form the composite (CPT), termed M-74 CPT@PTMSP, to improve moisture resistance and stability. Under the same MISA process, the new composite material achieved a regeneration energy consumption of only 1.29 MJ kg^{-1} CO_2 (≈45% lower than the commercial material) and maintained high cycling performance under wet conditions (Figure 7F). Furthermore, this material, with its highly coordinatively unsaturated metal sites, was demonstrated to have high CO_2 absorption capacity and high heating rate under ambient conditions. This series of optimizations has enabled MISA technology to move from laboratory concept verification to a stage closer to practical application.

Similarly, Li et al.[74] designed surface-functionalized magnetic nano-sorbents (nMAGs) by grafting polyethyleneimine (PEI) onto magnetite nanoparticles, enabling selective and recyclable CO_2 adsorption. These hybrid nanomaterials exhibited enhanced sorption capacity and superior magnetic separation capabilities, offering both performance and processability for CO_2 capture systems. Another approach involves magnetic MOF composites, where magnetic nanoparticles are integrated with MOF structures to achieve remote-triggered desorption. Li et al.[73] demonstrated that alternating magnetic fields effectively triggered CO_2 release from these composites through localized heating, thereby eliminating the need for direct thermal energy input. This strategy enhances energy efficiency by avoiding the bulk heating penalty associated with TSA. However, the CO_2 working capacity of MFCs is relatively low (e.g., $MgFe_2O_4$@UiO-66 exhibits only 1.8 wt%), which significantly limits their energy consumption performance per unit and results in overall energy efficiency that remains inferior to that of conventional absorbent systems. Additionally, the energy conversion efficiency of magnetic induction heating is highly sensitive to the loading of magnetic fillers, with conversion efficiency falling below 10% when particle loading is insufficient.

2.1.5. Pressure-Responsive Materials

Pressure-responsive materials exhibit structural flexibility that allows them to adapt their pore configurations or ligand conformations in response to external pressure as a stimulus.[75] This

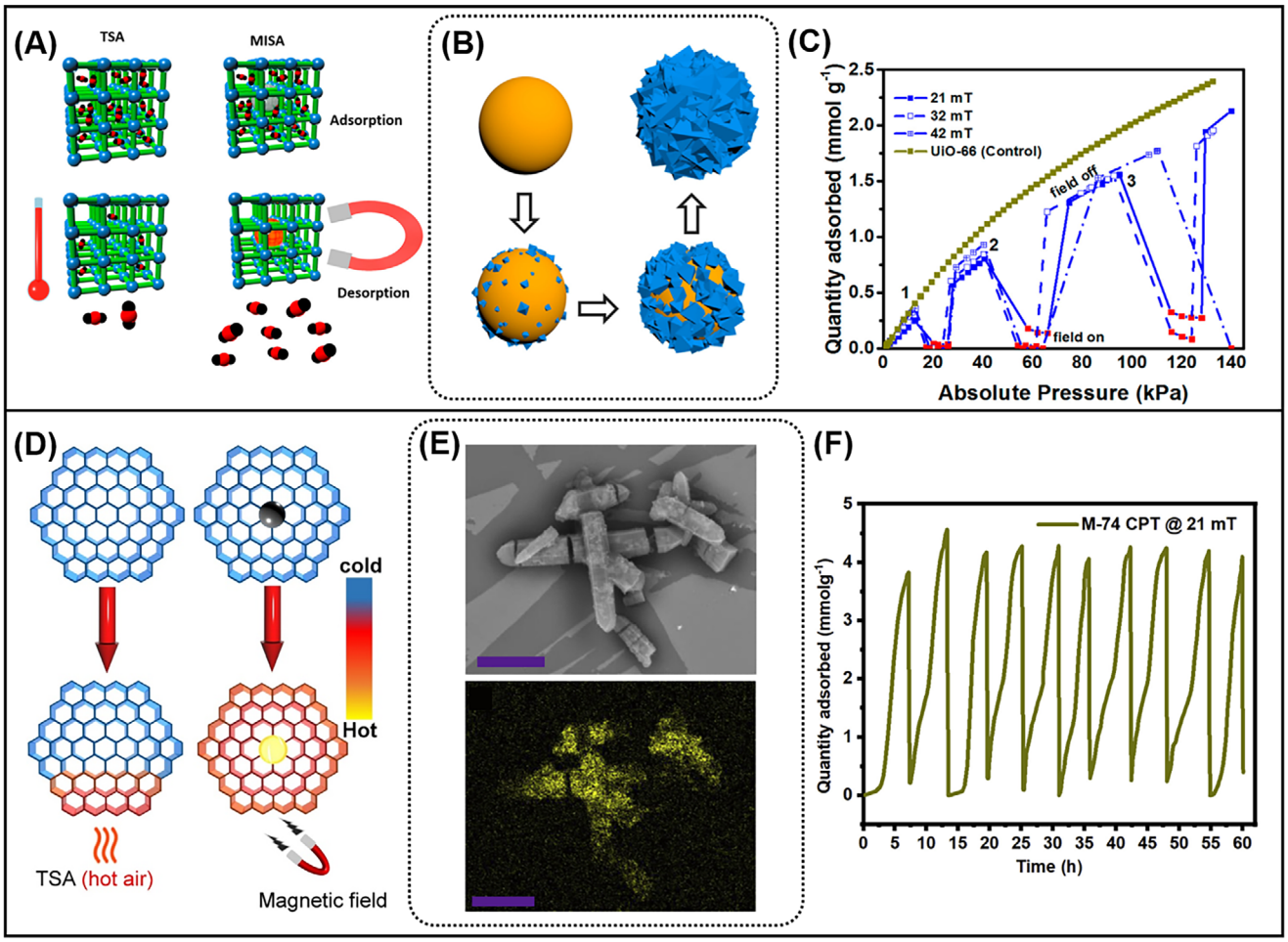

Figure 7. A) Demonstration of the maximal regeneration capability of magnetic framework composites (MFCs) through magnetic induction swing adsorption (MISA) as compared to conventional temperature swing adsorption (TSA). B) Scheme demonstrating the process of embedding $MgFe_2O_4$ nanospheres in a UiO-66 MOF. C) Dynamic uptake and release of CO_2 from MFC-mg2. Adapted with permission.[42] Copyright 2016, American Chemical Society. D) Comparison of Heat Transfer Mode between TSA and MISA in Adsorbents. E) SEM micrograph and elemental mapping of Fe atoms of M-74 CPT. Scale bar represents 5 µm. F) Dynamic uptake and release of CO_2 from M-74 CPT@21 mT (145 °C) and 0.15 kPa. Adapted with permission.[43] Copyright 2020, Elsevier.

unique responsiveness can significantly enhance CO_2 adsorption efficiency, especially under elevated pressures.

Hu et al.[45] investigated the well-known flexible MOF ZIF-8 and found that increasing external pressure induces subtle rotations of the imidazolate linkers, enlarging the pore apertures and facilitating CO_2 access. Through FTIR spectroscopy and molecular simulations, they confirmed that CO_2-framework interactions are strengthened under pressure, resulting in a gate-opening effect without structural collapse. The red shift in C = O stretching frequency under pressure further verified the enhanced binding between CO_2 and ZIF-8's framework. In a more complex system, Yuan et al.[46] developed PCN-69, a (3,24)-connected MOF built from a rigid, multi-nodal geodesic ligand (btti). This ligand exhibited pressure-induced curvature changes-shifting from a bent to a stretched conformation, which dynamically expanded the pore size in response to CO_2 pressure. This transformation was driven by covalent bond bending within the ligand, rather than conventional π-π-stacking or metal-ligand pivoting, representing a feasible mechanically responsive behavior on the molecular level. The resulting adsorption behavior showed stepwise and oscillatory patterns typical of structural transitions during gas loading and unloading. However, those materials may experience structural fatigue or pore collapse during repeated pressure cycling, which can negatively impact their operational lifespan and regeneration efficiency.

2.1.6. Redox-Responsive Materials

Redox active materials have emerged as promising candidates for controllable CO_2 capture and release under applied electrochemical stimuli.[76] These systems leverage redox-driven adsorption reactions, pH-swing mechanisms, or ion-insertion methods to achieve reversible, energy-efficient CO_2 separation.

The core of redox-responsive CO_2 capture lies in materials that reversibly respond to applied potentials, particularly redox-active organic compounds that show strong CO_2 affinity in their reduced states. Voskian and Hatton[41] pioneered the concept

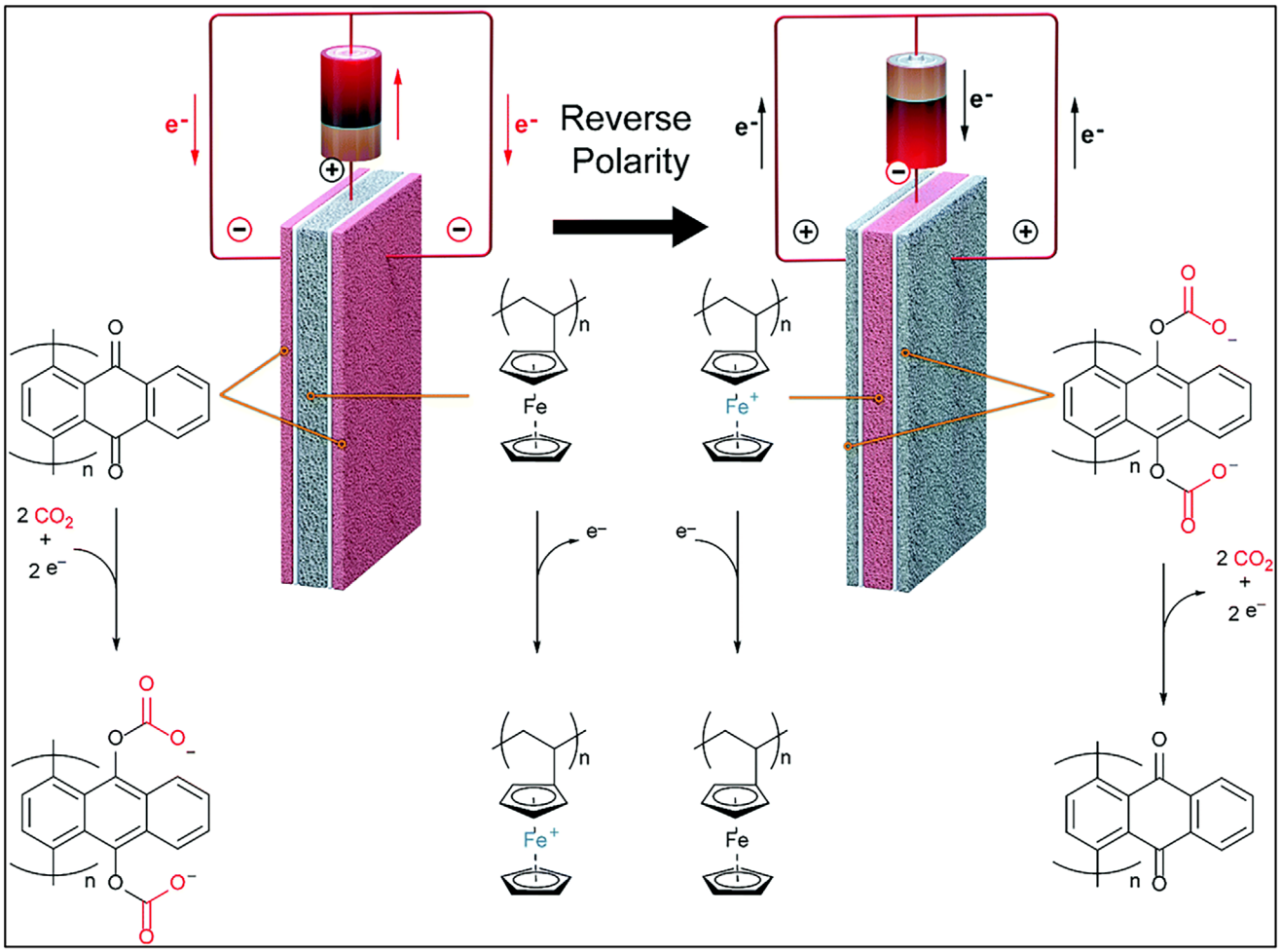

Figure 8. Schematic of a single electro-swing adsorption electrochemical cell with porous electrodes and electrolyte separators. The outer electrodes, coated with poly-1,4-anthraquinone composite, can capture CO_2 on application of a reducing potential via carboxylation of quinone, and release the CO_2 on reversal of the polarity. The inner polyvinylferrocene-containing electrode serves as an electron source and sink for the quinone reduction and oxidation, respectively. Adapted with permission.[44] Copyright 2019, RSC Publishing.

of "Faradaic Electro-Swing Adsorption" (FESA) (**Figure 8**), developing a solid-state capture device using a polyanthraquinone–carbon nanotube (PAQ-CNT) composite electrode. In this system, reduced quinone captures CO_2 via carboxylation, and subsequent oxidation releases it. The system demonstrated over 90% Faradaic efficiency and excellent cycling stability under various CO_2 concentrations, establishing the viability of this approach. Building on this, Iijima et al.[77] used in situ attenuated total reflectance–surface-enhanced infrared absorption spectroscopy (ATR-SEIRAS) spectroscopy and DFT calculations to investigate anthraquinone (AQ) and benzothiadiazole (BTZ) polymer electrodes under CO_2 atmospheres. They observed significant positive shifts in reduction potential in the presence of CO_2 and provided direct spectral evidence of CO_2 adsorption onto reduced redox units, confirming the simultaneous occurrence of one-electron reduction and CO_2 binding. From a molecular design perspective, Zito et al.[78] systematically analyzed the relationship between the reduction potential ($E_{1/2}$) and CO_2 binding constant (K_{CO2}) of various quinone derivatives, identifying a near-linear negative correlation. This implies that stronger CO_2-binding molecules typically have more negative reduction potentials, making them prone to oxygen reduction and deactivation—an electronic tradeoff that presents a key challenge in designing efficient and stable redox carriers.

Following the elucidation of redox-based mechanisms, structural design becomes crucial for improving system performance, especially in enhancing access to active sites and gas diffusion kinetics. Guo et al.[79] addressed limitations in CO_2 transport caused by excessive electrolyte wetting in conventional electrodes by designing Porous Polymeric Electrodes (PPEs). These were fabricated by anchoring redox-active units onto modified melamine foam, forming a 3D, gas-permeable framework that facilitates flow-through CO_2 capture. This design significantly improved the interfacial contact between the gas and the active material, minimized the diffusion distance, and achieved high material utilization (≈90%) and long-term stability. Taking a step further, Liu et al.[80] overcame the limited conductivity of polymer-based electrodes by employing a conductive metal organic framework (c-MOF), Ni_3(2,3,6,7,10,11-hexaiminotriphenylene)$_2$ (Ni_3(HITP)$_2$), and integrating electroactive nickel bis(diimine)

Table 1. Comparison of key performance metrics for representative stimuli-responsive CO_2 adsorbents.

Stimuli type	Representative material	CO_2 capacity [mmol g^{-1}]	Desorption energy [kJ mol^{-1}]	Recyclability (cycles)	Switching time [min]
Light	Ag/UiO-66,[60] DArE@PAF-1,[40] HCP-Azo[62]	0.92–2.65	low	5–10	4–60
Temperature	PNIPAM-*co*-CyclenZn,[66] SF-AM-*co*-NIPAM[47]	2.61–3.49	30–60	>5	-
Redox	PAQ–CNT,[41] Ni_3 $(HITP)_2$ MOF[80]	7.6–8.4	40–90	>100	≈10
Magnetism	M-74 CPT@PTMSP,[43] Fe_3O_4-MOF composites[42,73,74]	2.54–8.72	60–150	5–20	≈15
pH	PDEAMA microparticles,[44] UiO-66-SO_3H[69]	0.32–0.91	≈40	>10	≈45
Pressure	ZIF-8,[45] PCN-69[46]	2.5–4.0	Low (physical)	Several times	Instantaneous

(Ni-BDI) units directly into the framework. This enabled efficient solid-state electrochemical capture with high electronic conductivity and accessible surface area. The system exhibited excellent Faradaic efficiency, low energy consumption (30–72 kJ mol^{-1} CO_2), and robust tolerance to interfering gases like O_2 and NO_2, highlighting the importance of structural engineering in electrochemical CO_2 capture.

Beyond the conventional redox adsorption mechanisms, recent efforts have expanded the scope of electrochemical responsiveness to accommodate broader application scenarios and multifunctionality. Li et al.[81] introduced "charged-sorbents," where hydroxide ions were electrochemically injected into activated carbon pores. These OH^--loaded sorbents capture CO_2 via bicarbonate/carbonate formation and can be regenerated via low-temperature Joule heating (90–100 °C). This strategy bypasses the high-temperature calcination required in traditional DAC methods, offering a cost-effective and low-energy alternative suitable for atmospheric CO_2 removal. These advances illustrate the diversity of redox-responsive CO_2 capture strategies, ranging from redox-driven molecular binding to pH-swing and ion-based sorption. Although electrochemical CO_2 capture offers advantages in terms of energy efficiency and tunability, the organic redox-active molecules used (e.g., quinones) may suffer from decomposition or degradation during redox cycling, thereby compromising the long-term stability of the system. Moreover, their selectivity and resistance to interference from various gas impurities require further investigation.

2.1.7. Performance Comparison of Single-Responsive Materials

While different stimuli-responsive organic materials and polymers show promising CO_2 capture behavior, a direct performance comparison is essential to guide material selection. **Table 1** summarizes the adsorption capacity, energy consumption for desorption, recyclability and switching time of representative materials across various stimulus types.

Redox-responsive materials currently demonstrate the most balanced combination of CO_2 capture capacity, energy efficiency, and controllability. By reversibly modulating redox-active sites such as quinones, hydroxyls, or amines under low voltages (<1.5 V), these systems achieve high adsorption capacities (>5.0 mmol g^{-1}) and fast switching kinetics, making them particularly attractive for integration with electricity sources. Other stimuli-responsive systems, including those triggered by light, temperature, pH, magnetism, or pressure, offer unique advantages such as contactless control, compatibility with low-grade waste heat, or localized desorption. However, their application is often constrained by limitations in penetration depth, structural stability, working capacity, or scalability.

To overcome these respective shortcomings, the development of multi-stimuli-responsive systems represents a promising direction. Such hybrid designs can enhance adaptability to fluctuating operating conditions while improving responsiveness, selectivity, and process efficiency. Future work should also emphasize advanced materials engineering with a focus on structural stability at the molecular level, long-term cycling stability, and compatibility with regeneration strategies.

2.2. Multi-Responsive Materials

In the field of stimuli-responsive materials for CO_2 capture, both single-stimulus and multi-stimulus responsive systems exhibit unique advantages. Single-stimulus responsive materials are typically simple in terms of structure and molecular architecture, making them easy to design and regulate, and respond reversibly to individual external triggers. These systems often offer low energy consumption and good recyclability, making them suitable for simplified or energy-saving applications.[82] In contrast, multi-stimulus responsive materials can simultaneously respond to two or more external stimuli, offering greater control and adaptability in complex environments.[83] Thus, while single-stimulus systems are more suitable for low-energy, targeted use, multi-stimulus materials pave the way for advanced, intelligent CO_2 capture strategies.[36,84]

2.2.1. Redox- & pH-Responsive Materials

Although traditional thermal regeneration absorption methods (such as the amine washing methods) have been used for many

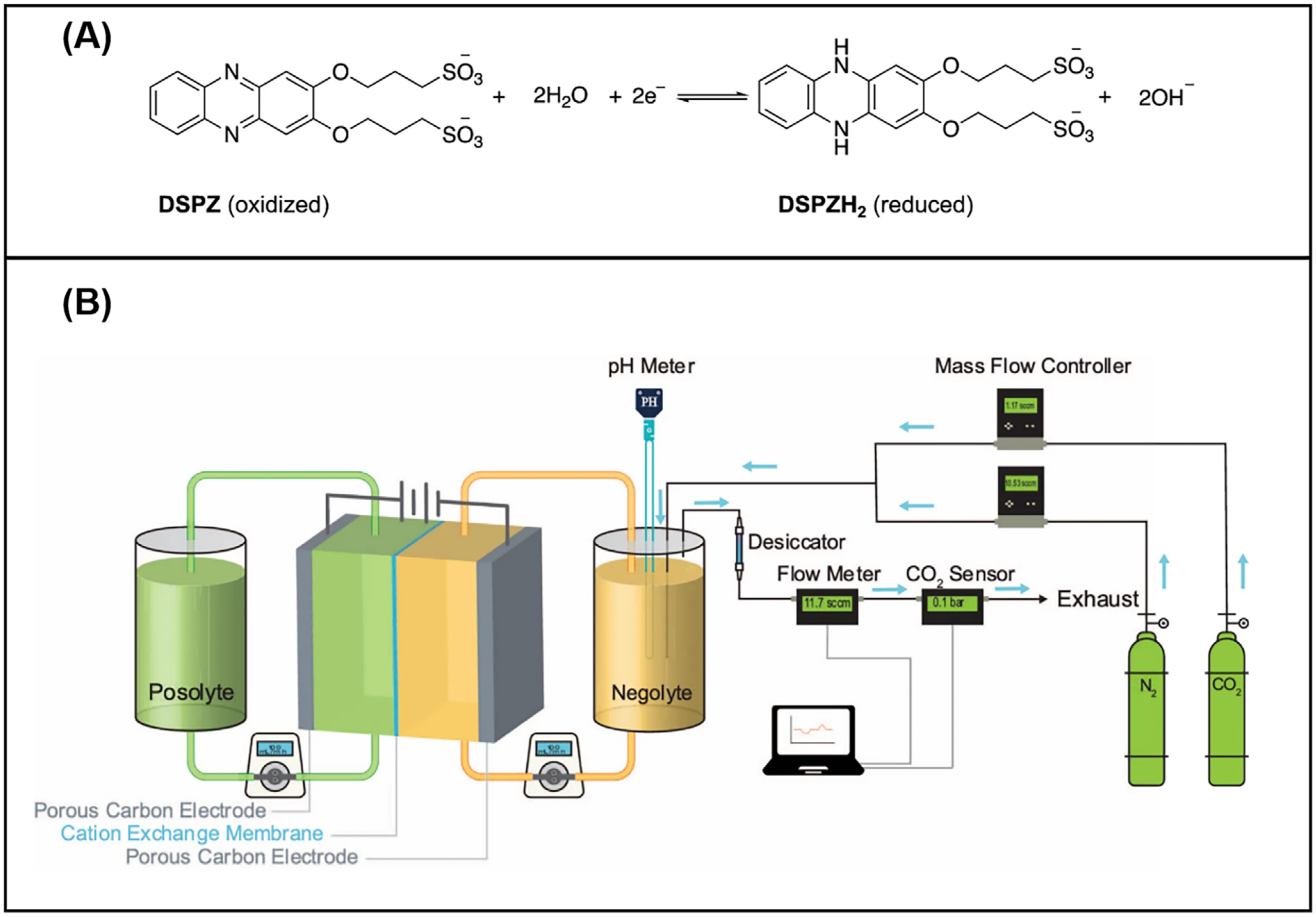

Figure 9. A) Schematic of the reversible PCET (proton-coupled electron transfer) reaction underwent by DSPZ (sodium (3,3′-(phenazine-2,3-diylbis(oxy))bis(propane-1-sulfonate))) in an aqueous solution. B) Schematic of the $Fe(CN)_6$ (posolyte) | DSPZ (negolyte) flow cell and full system. Blue arrows indicate gas flow direction. Adapted with permission.[88] Copyright 2022, Springer Nature.

years, they have problems such as high energy consumption, corrosiveness, and absorbent degradation.[85] In contrast, the electrochemically induced pH swing method has become an emerging alternative technology due to its high controllability, low temperature operation and adaptability to renewable energy[68,86] Organic molecular materials with dual response to pH and redox, especially water-soluble organic molecules working through the proton-coupled electron transfer (PCET) mechanism, have become the core research objects.[87]

Jin et al.[88] introduced a redox-active organic molecule, DSPZ (3,3′-(phenazine-2,3-diylbis(oxy))bis(propane-1-sulfonate)), which demonstrates efficient pH swing through PCET reactions (**Figure 9**). During electrochemical reduction, DSPZ increases the solution pH by generating hydroxide ions, thereby facilitating CO_2 absorption; subsequent oxidation releases protons, acidifying the solution and enabling CO_2 desorption. The system achieves an energy cost of 61.3 kJ mol^{-1} for CO_2 capture from 0.1 bar and extrapolates to 121–237 kJ mol^{-1} at ambient concentrations (0.4 mbar). However, DSPZ's reduced form is chemically sensitive to atmospheric oxygen, leading to electrolyte degradation and decreased cycle efficiency. To address this, the authors introduced a redox rebalancing method that restores the initial electrolyte state and prolongs device longevity.

In contrast, Pang et al.[89] developed 1,8-ESP (2,2′-(phenazine-1,8-diyl)bis(ethane-1-sulfonate)), a phenazine derivative engineered for optimized solubility and chemical stability. Unlike DSPZ, 1,8-ESP remains highly soluble in aqueous media across an exceptionally wide pH range (0–14.9), with concentrations exceeding 2.0 M. This results in a substantially higher CO_2 capture capacity-up to 1.48 mol L^{-1} at atmospheric levels and reduced energy consumption of 36–55 kJ mol^{-1}. Moreover, 1,8-ESP displays a good resistance to oxygen-induced degradation, with a capacity fade rate of less than 0.01% per day. Its low permeability and high surface tension also reduce membrane crossover and foaming, enhancing operational robustness. Notably, the system also enables dual functionality, coupling CO_2 capture with electrochemical energy storage, thus offering economic advantages in dynamic electricity markets through load balancing and carbon mitigation (**Figure 10**). Compared to traditional solvent-based CO_2 capture methods, such as MEA scrubbing, redox pH swing systems using responsive organic materials offer lower energy consumption (as low as 36–61 kJ mol^{-1} versus >100 kJ mol^{-1}), operate under ambient conditions, and avoid issues like corrosion, volatility, and toxicity. They enable fast, precise control via electricity rather than heat, making them compatible with renewable energy sources.

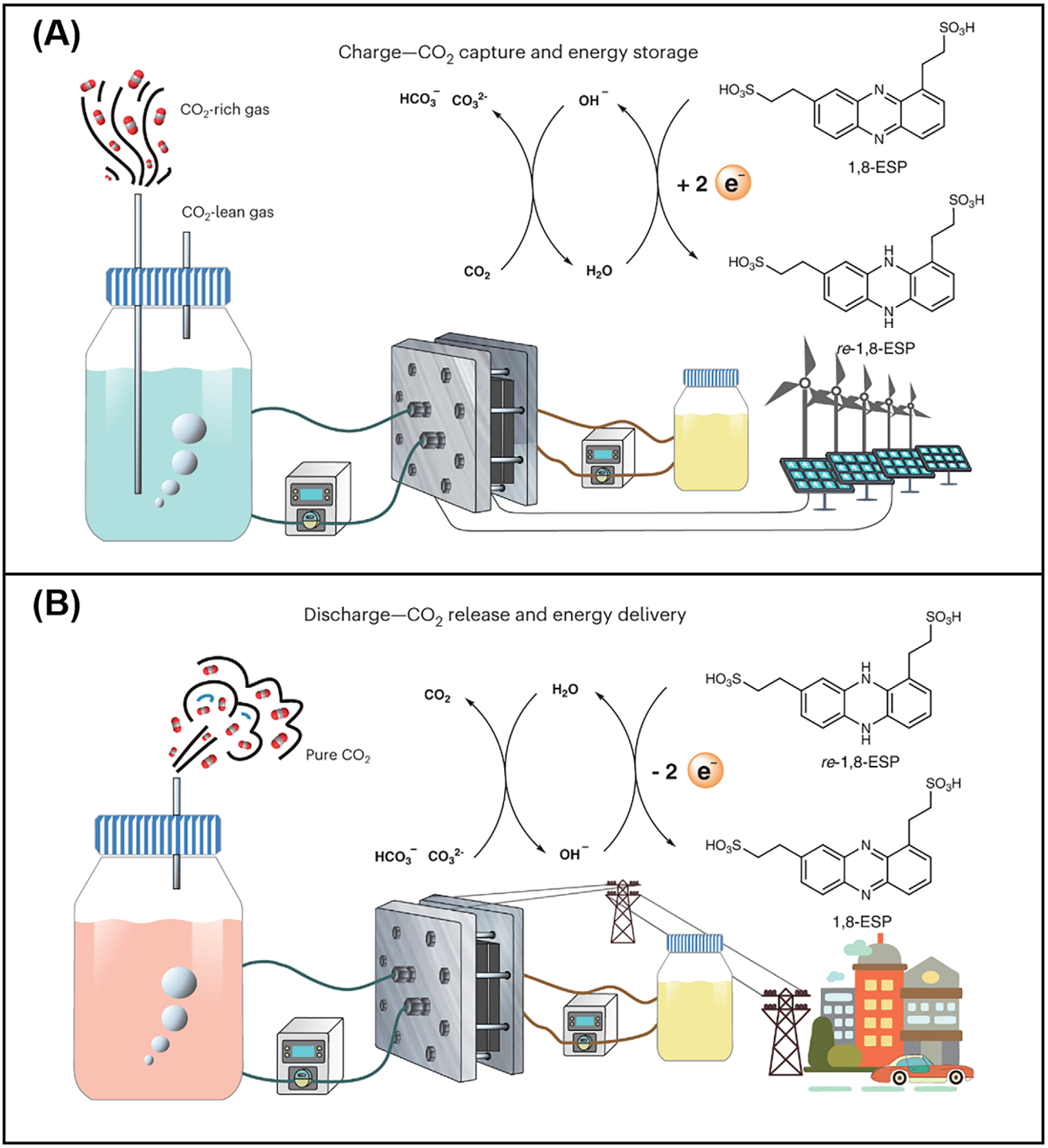

Figure 10. A) CO_2 capture and energy storage process. B) CO_2 release and energy delivery process. re-1,8-ESP is the reduced state of 1,8-ESP. Adapted with permission.[89] Copyright 2023, Springer Nature.

Compared to pH-responsive systems, dual-responsive systems enable precise control through the regulation of both current and potential. Although redox systems are inherently complex, the introduction of rebalancing techniques can mitigate oxygen interference and extend system lifespan. Despite the fact that the DSPZ system can achieve a low CO_2 separation energy of 61.3 kJ mol^{-1} at a current density of 20 mA cm^{-2}, maintaining high capture efficiency typically requires higher current densities. This leads to increased overpotentials and a rapid rise in energy consumption. Furthermore, when gas enters the liquid phase at low flow rates, the limited gas-liquid contact area results in low CO_2 absorption efficiency. Therefore, improvements

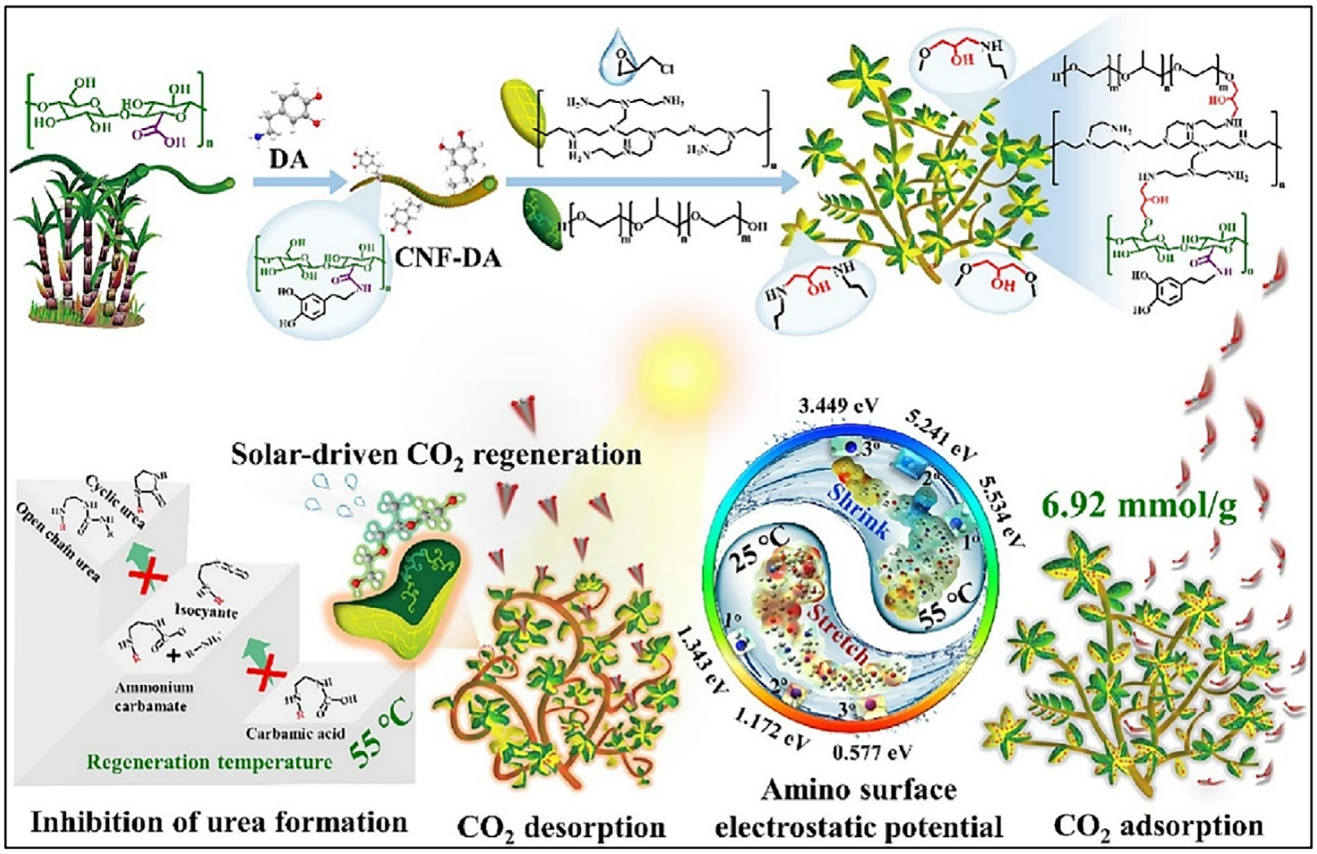

Figure 11. Preparation and application of the solar-driven regenerable photothermal responsive cellulose carbon capture material. Adapted with permission.[100] Copyright 2024, Elsevier.

should incorporate contactor design strategies to enhance the interfacial area between gas and liquid phases.

2.2.2. Light- & Temperature-Responsive Materials

Light- and temperature-responsive materials have been explored as a novel class of switchable CO_2 adsorbents. By incorporating photoisomerizable moieties or thermally reactive groups into porous frameworks, these materials enable reversible control over gas adsorption behaviors through external stimuli, offering new pathways for low-energy CO_2 capture and release.[59,90]

Luo et al.[91] developed a light- and temperature-responsive cellulose-based carbon capture material (PTCCM) by crosslinking light- and temperature- cellulose nanofibers (CNF-DA), the thermosensitive polymer Pluronic F-127, and polyethyleneimine (PEI), resulting in a multi-network structure with a high amine density (14.18 mmol g^{-1}) and excellent CO_2 adsorption capacity (6.92 mmol g^{-1}) (**Figure 11**). Upon heating, the contraction of F-127 molecular chains increases the surface potential and passivates the amine groups, enabling low-temperature regeneration at just 55 °C for more than 10 times with a 92.05% regeneration rate. In a separate study, Park et al.[92] synthesized a light/temperature-responsive MOF by incorporating azobenzene moieties into the organic linkers, enabling light-induced cis-trans isomerization to trigger reversible changes in pore structure and thereby regulate CO_2 adsorption behavior. This MOF, designated PCN-123, exhibited a significant decrease in CO_2 uptake from 22.9 to 10.5 cm^3 g^{-1} under UV irradiation with a 53.9% reduction. Upon thermal treatment at 60 °C, the adsorption capacity was nearly restored to its original level, indicating excellent structural and functional reversibility. The stimulus-responsive mechanism relies on pore size modulation and the accessibility of primary adsorption sites driven by azobenzene isomerization. This study represents the first demonstration of photoinduced structural transformation in a MOF to modulate gas adsorption capacity.

Compared to materials with single light- or temperature-responsiveness, light/temperature-responsive CO_2 adsorbents significantly reduce regeneration energy consumption through synergistic photothermal effects. The F-127 achieves efficient regeneration at just 55 °C, outperforming conventional temperature-responsive materials that require higher temperatures. Additionally, such materials exhibit faster response rates, higher adsorption capacities (up to 6.92 mmol g^{-1}), and good stability during cycling. However, they also face challenges such as complex structures and relatively high production costs. Moreover, the light-responsive component is still limited by irradiation conditions, which requiring further optimization for practical applications.

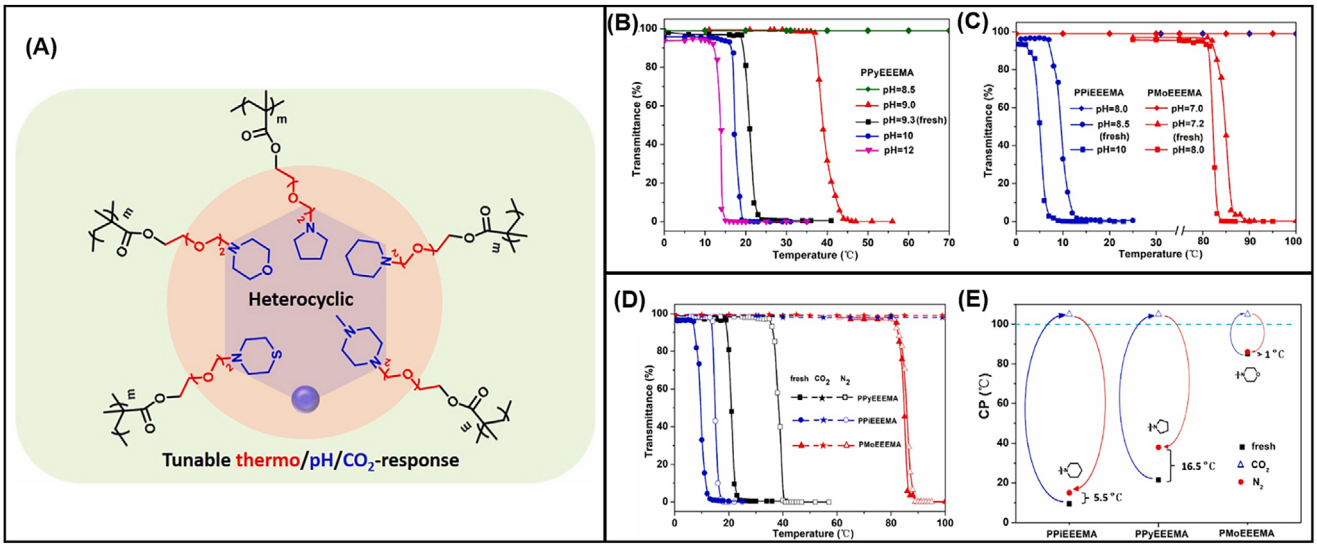

Figure 12. A) Structure of the multi-responsive polymers for CO_2 capture strategies. B) pH effect on the thermo-responsiveness of 1.0 wt% poly((pyrrolidineethoxyethyl methacrylate)-*co*-poly(acrylic acid)) ($PPyEEEMA_{72}$) aqueous solution and C) poly((piperidine ethoxyethyl methacrylate)-*co*-poly(acrylic acid)) ($PPiEEEMA_{77}$) and poly((morpholine ethoxyethyl methacrylate)-*co*-poly(acrylic acid)) ($PMoEEEMA_{81}$) aqueous solution. Note: "fresh" means that the aqueous solution of the polymer is freshly prepared. Thermoresponse of 1.0 wt% aqueous solutions of $PPyEEEMA_{72}$, $PPiEEEMA_{77}$ and poly((*N*-methylpiperazineethoxyethyl methacrylate)-*co*-poly(acrylic acid)) ($PMPiEEEMA_{71}$) under D) CO_2/N_2 bubbling and E) a summary of CPs. Adapted with permission.[95] Copyright 2023, Elsevier.

2.2.3. Temperature- & pH-Responsive Materials

pH- and temperature-responsive polymers have gained attention as dynamic materials for CO_2 capture due to their ability to reversibly alter conformation, solubility, or porosity in response to environmental changes.[67,93] Such systems enable externally tunable adsorption behaviors via synergistic effects between thermal transitions and protonation/deprotonation processes.[94]

Wang et al.[95] synthesized a new family of multi-stimuli-responsive acrylamide-based homopolymers bearing heterocyclic substituents to investigate how molecular structure influences the thermo/pH/CO_2-responsiveness (**Figure 12A**). These polymers exhibit distinct lower critical solution temperature (LCST) characteristics in aqueous solutions, which can be tuned by molecular weight, concentration, and salt content. They also demonstrate upper critical solution temperature (UCST) behavior in certain alcoholic solvents, indicating strong solvent sensitivity. Regarding pH-responsiveness, the critical pH varies with the initial pH and temperature of the solution, and pH changes can modulate LCST (Figure 12B,C). As pH increases, hydrophobicity strengthens and LCST decreases, confirming a coupled thermal and pH response. The polymers become fully soluble upon CO_2 bubbling due to the formation of hydrophilic ammonium bicarbonates, resulting in the disappearance of the LCST. After nitrogen purging, partial recovery of the LCST occurs, with the extent and rate influenced by the basicity of the amine group (Figure 12D,E). These findings underscore the pivotal role of heterocyclic substituents in modulating the multi-responsive properties of polymers, offering valuable insights for designing advanced smart polymer systems. This research group also reported the development of a triple-responsive polymer series where CO_2 sorption further modulates pH and temperature responsiveness.[96] CO_2 bubbling increased solubility by forming ionic carbamate species, while removal of CO_2 restored the original hydrophobicity and LCST behavior. These polymers exhibited tunable cloud point (CP) behaviors under varying degrees of polymerization (DP), concentrations, and the presence of salts, revealing the designability of dual (and triple) stimuli responsiveness for smart capture systems.

Compared to polymers with only pH or temperature responsiveness, these materials exhibit broader environmental adaptability and greater tunability. The synergistic effects between stimuli allow precise control over solubility and phase transition behavior through multiple external triggers. However, these materials still face challenges, including complex synthesis routes and slow recovery after CO_2 exposure.

2.2.4. Pressure- & Temperature-Responsive Materials

Pressure- and temperature-responsive porous materials offer a promising strategy for tunable CO_2 capture by leveraging external physical stimuli to induce framework flexibility, pore transformation, or modulation of adsorption affinity.[97] These systems exhibit reversible structural transitions or shifts in adsorption isotherms under coupled pressure-temperature fields, providing pathways for energy-efficient control of gas sorption.[98]

Liu et al.[99] studied MIL-53(Al), a flexible MOF known for its breathing behavior, and demonstrated enhanced CO_2 adsorption through cooperative pressure and temperature modulation (**Figure 13A**). In situ X-ray diffraction and molecular simulations revealed that at room temperature and CO_2 pressure below 0.2 bar, MIL-53(Al) remained in a narrow-pore (np) phase. However, increasing pressure beyond this threshold triggered a phase transition to the large-pore (lp) form, which accommodated more CO_2 molecules. Temperature played a critical role

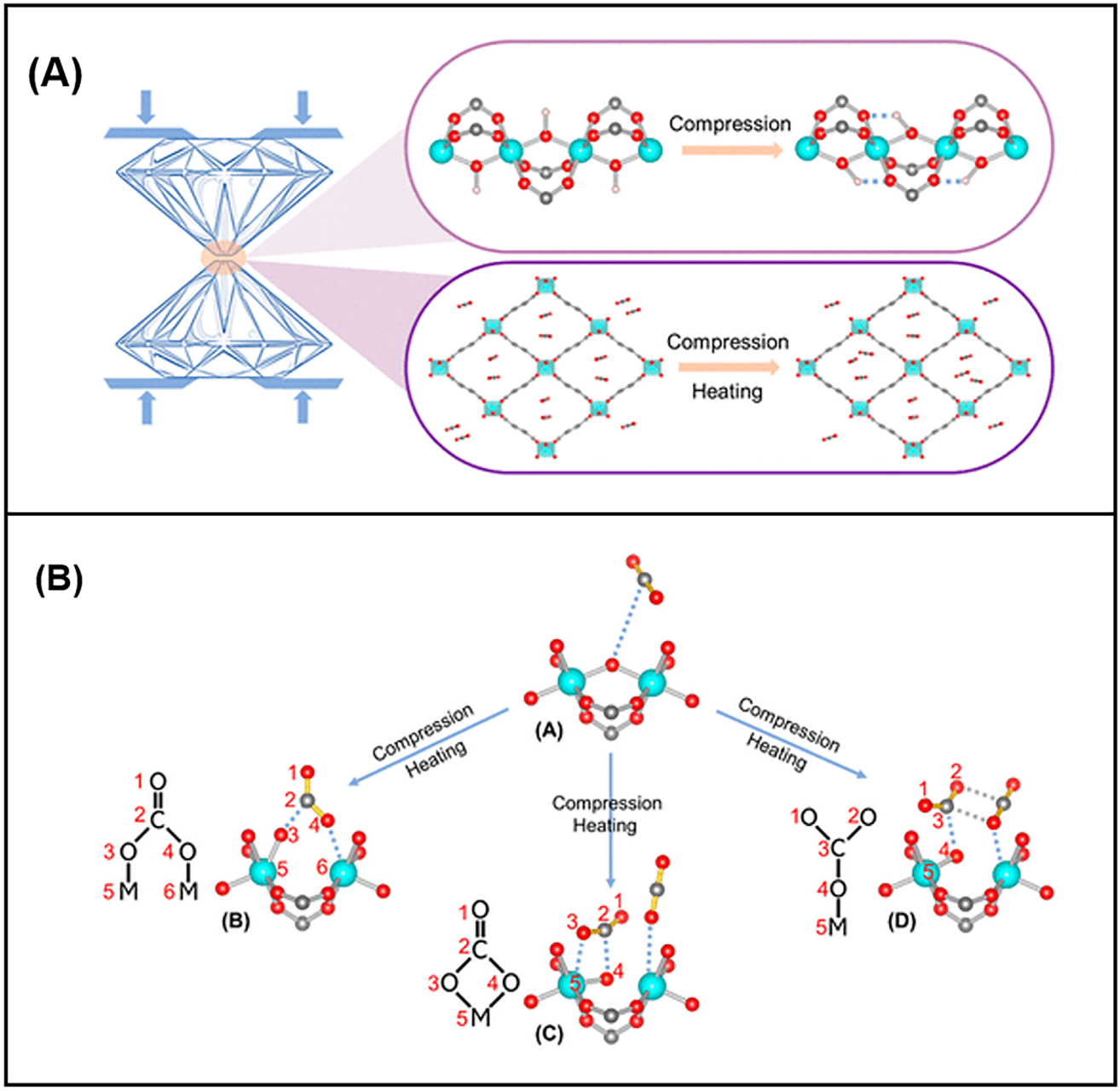

Figure 13. A) Schematic illustrations of MIL-53(Al). B) Schematic illustrations of the transition process of the possible manners of host–guest interactions in CO_2@MIL-53(Al) at high pressures and high temperature. Color coding: Al, blue; O, red; C, gray. The hydrogen atoms are omitted. Adapted with permission.[99] Copyright 2024, American Chemical Society.

in modulating the transition pressure: at elevated temperatures (e.g., 353 K), the lp phase was stabilized at higher CO_2 pressures, whereas at lower temperatures (e.g., 273 K), the lp phase was facilitated even at reduced pressures. Notably, CO_2 uptake peaked near the np→lp transition point, where guest-induced framework expansion maximized adsorption enthalpy and entropy (Figure 13B), highlighting the synergy of temperature and pressure in tuning sorption. These findings underscore the potential of pressure- and temperature-coupled MOFs for CO_2 capture systems with switchable porosity, offering adjustable gas sorption profiles through physical stimuli rather than chemical regeneration.

Compared to materials with single pressure or temperature responsiveness, the MIL-53(Al) system demonstrates superior CO_2 adsorption performance through synergistic pressure-temperature modulation. This dual-stimulus approach enhances adsorption capacity and selectivity by effectively triggering the material's "breathing" structural transitions, which is hard to realize under a single stimulus. However, the system has a narrow operating window at low temperatures and moderate pressures,

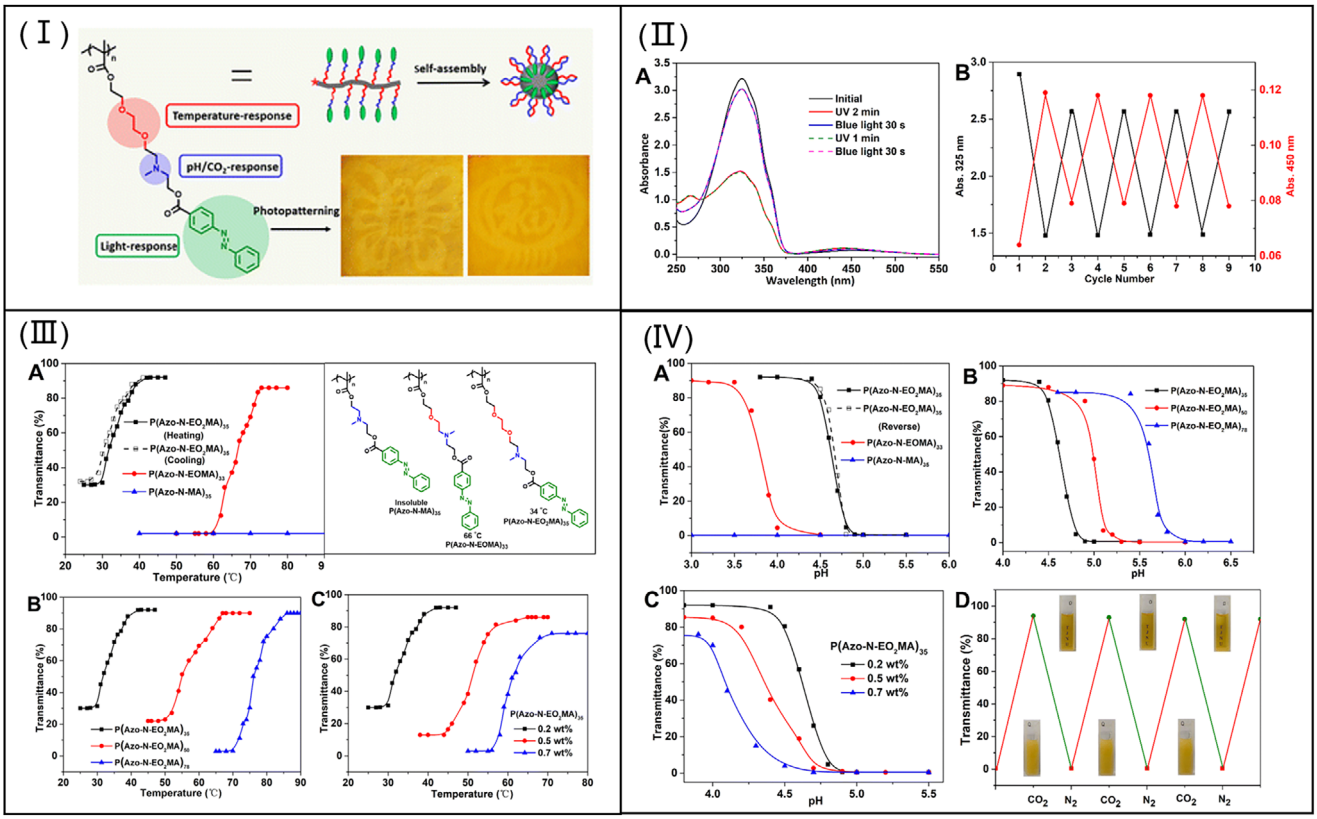

Figure 14. I) Schematic illustrations of light/temperature/pH/CO_2-quadruple responsive azobenzene functionalized homopolymer of P(Azo-*N*-EO_2MA). II) UV–vis absorption spectra of P(Azo-*N*-EO_2MA)$_{35}$ in THF solution (0.1 mg mL^{-1}) under A) irradiation with UV/blue light and reversible absorbance changes under B) alternating UV and blue light irradiation. III) Thermoresponsiveness of P(Azo-*N*-EO_2MA)$_{35}$, P(Azo-*N*-EOMA)$_{33}$ and P(Azo-*N*-MA)$_{35}$ in ^{n}BuOH/H_2O (H_2O wt% = 15%, C = 0.2 wt%) and their structures (A). Effect of DP (B) and concentration (C) on the thermoresponsiveness of P(Azo-*N*-EO_2MA)$_{35}$. (IV) The pH-dependent transmittance of P(Azo-*N*-EO_2MA)$_{35}$, P(Azo-*N*-EOMA)$_{33}$ and P(Azo-*N*-MA)$_{35}$ (0.2 wt%) (A) and the effect of DP (B) and concentration (C) on the pH-responsiveness of P(Azo-*N*-EO_2MA)$_{35}$. Transmittance changes of an aqueous solution of P(Azo-*N*-EO_2MA)$_{35}$ (1 mg mL^{-1}) upon bubbling with CO_2/N_2 (D). Adapted with permission.[100] Copyright 2024, RSC Publishing.

resulting in a slow structural response. These factors constrain its immediate practical application.

2.2.5. Light-, pH- & Temperature-Responsive Materials

Poly((E)-3,14-dimethyl-13-oxo-6,9,12-trioxa-3-azapentadec-14-en-1-yl4 (phenyldiazenyl)benzoate) (P(Azo-N-EO_2MA)) is an azobenzene-functionalized homopolymer synthesized via RAFT polymerization that exhibits triple responsiveness to light, temperature, and pH, making it highly promising for controllable CO_2 capture and release applications.[100] The polymer incorporates amine, ethoxy, and azobenzene groups, each imparting specific responsiveness to pH, temperature, and light, respectively (**Figure 14**I). In terms of CO_2 responsiveness, the amine groups react with CO_2 in aqueous solution to form ammonium bicarbonate, leading to a pH drop and subsequent protonation of the polymer. This protonation causes the polymer to transition from a hydrophobic, insoluble state to a hydrophilic, soluble state. Experimental results showed that bubbling CO_2 into a solution of P(Azo-N-EO_2MA) at an initial pH of 6.6 led to a rapid phase transition from turbid to clear within 1 min, with transmittance increasing from 1.5% to 95% (Figure 14IV). This process was fully reversible through nitrogen purging, demonstrating a robust CO_2-triggered solubility switch.

Regarding temperature responsiveness, P(Azo-*N*-EO_2MA) exhibits upper critical solution temperature (UCST) behavior in an *n*-butanol/water co-solvent system. Its UCST can be finely tuned by modifying the polymer's hydrophobicity, degree of polymerization (DP), and concentration. For instance, increasing DP resulted in UCST shifts from 34 to 76 °C, enabling tailored CO_2 absorption thresholds across a range of conditions (Figure 14III). In certain acidic buffer environments, the polymer also displayed LCST-type transitions, indicating a versatile thermal response range that can be exploited for temperature-regulated gas sorption. The polymer's light- responsiveness is derived from the trans–cis photoisomerization of azobenzene groups under UV and blue light irradiation. This structural change alters the polymer's polarity and hydrophilicity, indirectly modulating both the UCST and critical pH. For example, UV irradiation reduced the UCST from 34 to 25 °C and increased the critical pH from 4.65 to 5.0, while subsequent blue light exposure partially restored the original values (Figure 14II). Light, therefore, acts as a non-invasive and reversible external trigger to tune the polymer's solubility and CO_2-responsiveness.

The interplay among pH, temperature, and light responses creates a highly programmable CO_2 capture platform. pH triggers directly drive CO_2-induced solubility switching, temperature sets the phase transition window, and light allows fine-tuning of system thresholds, enabling a "light-temperature-pH" logic control over CO_2 absorption behavior. Although this study does not focus on carbon capture, the light/pH/temperature triple-responsive supramolecular polymer system it presents demonstrates notable advantages over single-stimulus systems, including enhanced controllability, reversible and sequential responses, and increased adaptability to external conditions. However, its CO_2 responsiveness is indirectly triggered by pH changes rather than specific adsorption, and the system lacks porosity or active sites necessary for actual CO_2 capture. Therefore, while the material design is innovative in its stimuli-responsive properties, it is not inherently suitable for practical carbon capture without structural and functional modifications.

2.2.6. Redox-, pH- & Temperature-Responsive Materials

Redox-, pH- and temperature-responsive organic materials offer multi-dimensional control over CO_2 capture performance by integrating redox-active centers, protonation sites, and temperature-responsive backbones into a single platform.[86,101] The multifunctional system can adapt conformation, solubility, and charge under varied stimuli, enabling on-demand gas adsorption and release via external environmental or electrochemical inputs.[102]

Wang et al.[103] designed a series of ferrocene-containing homopolymers (PFcEEEMAs) that exhibit quadruple-responsiveness to CO_2, redox (electrochemical), pH, and temperature as external triggers. By incorporating hydrophobic ferrocene (Fc) units with hydrophilic ethoxy chains and tertiary amine groups into a single monomer structure, a balance between structural simplicity and multi-responsiveness can be achieved. These homopolymers were synthesized via RAFT polymerization, allowing for precise control over molecular weight and architecture. The polymers demonstrated an upper critical solution temperature behavior in alcohol solvents, where the cloud point could be tuned by chain length, molecular weight, and concentration. In aqueous solution, the polymers exhibited clear pH-responsiveness, with the critical pH value adjustable through structural variation. As shown in **Figure 15B**, when CO_2 is bubbled into a turbid aqueous solution of $P(Fc\text{-}N\text{-}EO2MA)_{47}$, the tertiary amine groups react with carbonic acid (formed from CO_2 and water) to generate ammonium bicarbonate. This significantly enhances the polymer's hydrophilicity, causing the solution to become transparent within 30 s. The process is fully reversible: subsequent bubbling of N_2 removes CO_2, leading to reprecipitation of the polymer and a return to turbidity.

The redox-responsiveness of the polymers arises from the reversible oxidation of Fc to hydrophilic Fc^+ by $FeCl_3$ and reduction back to Fc by vitamin C, which alters both solubility and self-assembly behavior. In aqueous media, the polymers form micelles with morphologies such as spheres or lamellae, which respond dynamically to stimuli. $P(Fc\text{-}N\text{-}EOMA)_{48}$ micelles swell under acidic conditions and further loosen upon Fc oxidation, while base or reductant treatment restores their original structure, demonstrating fully reversible morphological control (Figure 15A). However, since CO_2 only acts as a pH regulator rather than a target for capture, the system lacks actual testing of its CO_2 capture capabilities. Although the material design is innovative in terms of responsive behavior, structural and functional modifications suitable for CO_2 capture are still needed as the same strategy in *2.2.5*.

3. Conclusions and Outlook

This review has comprehensively summarized recent advances in stimuli-responsive organic materials and polymers for CO_2 capture. By analyzing the mechanisms and representative systems of six primary external stimuli such as light, temperature, pH, redox, magnetism, and pressure, we highlight how these materials enable reversible and controllable CO_2 adsorption and desorption. In particular, redox-responsive and multi-stimuli systems stand out due to their high tunability, energy efficiency, and potential integration into electrochemical or hybrid energy systems, making them promising for intelligent carbon capture.

3.1. Summary of Main Achievements

These stimuli-responsive CO_2 absorbers have various accomplishments: (1) Stimuli-responsive materials allow on-demand adsorption and desorption, enabling energy-efficient regeneration and system modularity. (2) Many systems, especially COFs and MOFs with functionalized organic linkers, demonstrate excellent CO_2/N_2 selectivity, making them attractive for post-combustion applications. (3) Electrochemical and photothermal capture approaches provide a direct route for coupling carbon capture with solar, wind, or waste heat, enhancing system sustainability. (4) Researchers have developed responsive frameworks using bio-derived polymers, ionic sites, supramolecular systems, and engineered living materials, offering a broad design landscape.

3.2. Critical Challenges and Limitations

Despite their promising potential, several critical challenges persist: (1) Complex synthesis routes and costly functionalization hinder large-scale translation. (2) Stability and recyclability remain problematic for light- and redox-active systems under repeated cycling or harsh flue gas environments. (3) Coupled stimuli may interfere with one another, requiring deeper investigation into synergistic or competitive effects. (4) Most studies remain at the laboratory scale, with limited assessment of mass transfer efficiency, lifecycle performance, or process integration.

3.3. Future Research Directions

To address these challenges, future research should prioritize the following directions: (1) Eco-friendly synthesis, leveraging renewable building blocks and solvent-free chemistry for sustainable material production. (2) Combine responsive materials

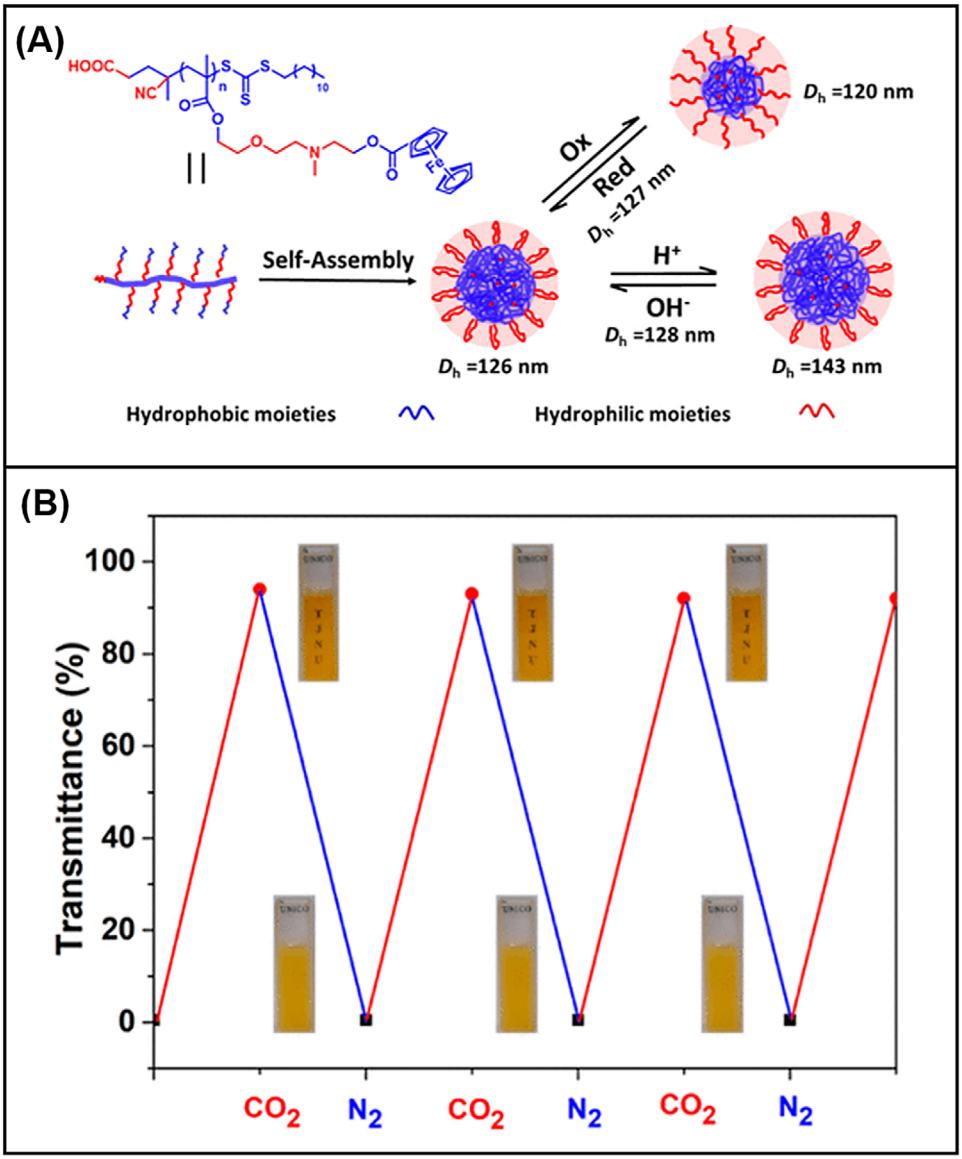

Figure 15. A) Schematic diagram of the evolution process of the morphology and D_h of P(Fc-*N*-EOMA)$_{48}$ micelles under different stimuli. B) Transmittance changes of aqueous solution of P(Fc-*N*-EO$_2$MA)$_{47}$ (0.5 wt%) upon the CO_2/N_2 bubbling. Adapted with permission.[103] Copyright 2023, American Chemical Society.

with membrane modules, electrochemical cells, or adsorption reactors for hybrid capture systems. (3) Application-specific engineering, tailoring material properties for DAC, post-combustion, biogas upgrading or modular CO_2 storage applications. (4) Expanding the development of redox-responsive systems and multi-stimuli-responsive materials incorporating electricity due to the rapid response and precise controllability of electric stimuli.

3.4. Potential Application Scenarios

Additionally, it is necessary to explore the application scenarios of different stimuli-responsive materials to translate these innovations from the laboratory to practical applications. (1) Redox-responsive systems such as quinone-based flow cells can be integrated into solar- or wind-powered DAC units in remote energy farms. (2) Light- and temperature-responsive adsorbents could be applied as dynamic coatings on building facades, passively capturing and releasing CO_2 in sync with sunlight and ambient heat. (3) Multi-stimuli-responsive micelles or hydrogels show promise in wearable or compact air filtration devices, particularly for personalized carbon management or space exploration. (4) Magnetic-responsive materials can facilitate rapid, remote regeneration in rotating bed reactors or continuous flue gas treatment under harsh industrial conditions. (5) Future CO_2-energy coupled systems may simultaneously capture CO_2 and store/release energy.

By combining these stimuli-responsive materials with specific application environments, the scope of CO_2 capture will be greatly expanded. With continued interdisciplinary innovation and engineering integration, stimuli-responsive organic materials and polymers are expected to provide scalable, low-energy and intelligent solutions for climate change mitigation and carbon neutrality.

Acknowledgements

The authors thank the Saarland state government, within the framework of the Saarland Transformation Fund ENFOSAAR, for funding and support of this study.

Open access funding enabled and organized by Projekt DEAL.

Conflict of Interest

The authors declare no conflict of interest.

Keywords

carbon capture, global warming, multi-stimuli systems, smart adsorption–desorption, stimuli-responsiveness

Received: August 10, 2025
Revised: September 15, 2025
Published online: September 29, 2025

[1] a) M. T. McCulloch, A. Winter, C. E. Sherman, J. A. Trotter, *Nat. Clim. Change* **2024**, *14*, 171; b) J. E. Hansen, M. Sato, L. Simons, L. S. Nazarenko, I. Sangha, P. Kharecha, J. C. Zachos, K. von Schuckmann, N. G. Loeb, M. B. Osman, Q. Jin, G. Tselioudis, E. Jeong, A. Lacis, R. Ruedy, G. Russell, J. Cao, J. Li, *Oxford Open Clim. Change* **2023**, *3*, kgad008.

[2] World Meteorological Organization, *WMO confirms 2024 as warmest year on record at about 1.55 °C above pre-industrial level*, **2025**, https://wmo.int/news/media-centre/wmo-confirms-2024-warmest-year-record-about-155degc-above-pre-industrial-level.

[3] a) World Meteorological Organization, *Greenhouse gases* **2025**, https://wmo.int/topics/greenhouse-gases; b) N. James, M. Menzies, *Physica A* **2022**, *608*, 128302.

[4] a) F. M. Santos, A. L. Gonçalves, J. C. Pires, in *Bioenergy with Carbon Capture And Storage*, Elsevier, Amsterdam, Netherlands, **2019**, p. 1; b) R. S. Haszeldine, S. Flude, G. Johnson, V. Scott, *Philos. Trans. R. Soc., A* **2018**, *376*, 20160447.

[5] a) L. Chen, G. Msigwa, M. Yang, A. I. Osman, S. Fawzy, D. W. Rooney, P.-S. Yap, *Environ. Chem. Lett.* **2022**, *20*, 2277; b) S. Yang, D. Yang, W. Shi, C. Deng, C. Chen, S. Feng, *Environ. Sci. Pollut. Res.* **2023**, *30*, 81725; c) Y. Zhang, C.-L. Pan, H.-T. Liao, *Front. Environ. Sci.* **2021**, *9*, 761736; d) X. Zhao, X. Ma, B. Chen, Y. Shang, M. Song, *Resour. Conserv. Recycl.* **2022**, *176*, 105959.

[6] Intergovernmental Panel on Climate Change (IPCC), *Contribution of Working Groups I, II and III to the Sixth Assessment Report of the Intergovernmental Panel on Climate Change*, IPCC, Geneva, Switzerland **2023**. Available at: https://www.ipcc.ch/report/ar6/syr/downloads/report/IPCC_AR6_SYR_SPM.pdf.

[7] a) N. Bahman, M. Al-Khalifa, S. Al Baharna, Z. Abdulmohsen, E. Khan, *Rev. Environ. Sci. Bio/Technol.* **2023**, *22*, 451; b) B. Dziejarski, R. Krzyżyńska, K. Andersson, *Fuel* **2023**, *342*, 127776.

[8] K. S. Lackner, *Eur. Phys. J. Spec. Top.* **2009**, *176*, 93.

[9] a) M. E. Boot-Handford, J. C. Abanades, E. J. Anthony, M. J. Blunt, S. Brandani, N. M. Dowell, J. R. Fernández, M.-C. Ferrari, R. Gross, J. P. Hallett, *Energy Environ. Sci.* **2014**, *7*, 130; b) J. Gibbins, H. Chalmers, *Energy Policy* **2008**, *36*, 4317; c) A. Raza, R. Gholami, R. Rezaee, V. Rasouli, M. Rabiei, *Petroleum* **2019**, *5*, 335.

[10] a) M. Bui, C. S. Adjiman, A. Bardow, E. J. Anthony, A. Boston, S. Brown, P. S. Fennell, S. Fuss, A. Galindo, L. A. Hackett, *Energy Environ. Sci.* **2018**, *11*, 1062; b) J. C. Pires, F. G. Martins, M. C. Alvim-Ferraz, M. Simões, *Chem. Eng. Res. Des.* **2011**, *89*, 1446.

[11] D. Moreira, J. C. Pires, *Bioresour. Technol.* **2016**, *215*, 371.

[12] a) W. Gao, S. Liang, R. Wang, Q. Jiang, Y. Zhang, Q. Zheng, B. Xie, C. Y. Toe, X. Zhu, J. Wang, *Chem. Soc. Rev.* **2020**, *49*, 8584; b) X. Y. D. Soo, J. J. C. Lee, W.-Y. Wu, L. Tao, C. Wang, Q. Zhu, J. Bu, *J. CO2 Util.* **2024**, *81*, 102727.

[13] M. C. Romano, P. Chiesa, G. Lozza, *Int. J. Greenhouse Gas Control* **2010**, *4*, 785.

[14] F. Raganati, F. Miccio, P. Ammendola, *Energy Fuels* **2021**, *35*, 12845.

[15] a) N. E. Flø, H. Knuutila, H. M. Kvamsdal, M. Hillestad, *Int. J. Greenhouse Gas Control* **2015**, *41*, 127; b) S. Laribi, L. Dubois, G. De Weireld, D. Thomas, *Int. J. Greenhouse Gas Control* **2019**, *90*, 102799; c) M.-H. Chang, W.-C. Chen, C.-M. Huang, W.-H. Liu, Y.-C. Chou, W.-C. Chang, W. Chen, J.-Y. Cheng, K.-E. Huang, H.-W. Hsu, *Energy Procedia* **2014**, *63*, 2100.

[16] X. Huang, N. Ai, L. Li, Q. Jiang, Q. Wang, J. Ren, J. Wang, *Separations* **2022**, *9*, 95.

[17] a) G. S. Kumar, M. Viswandham, A. Gupta, G. S. Kumar, *Int. J. Res. Eng. Technol* **2013**, *2*, 847; b) H. Liu, Y. Shao, *Appl. Energy* **2010**, *87*, 3162; c) A. Mukherjee, J. A. Okolie, A. Abdelrasoul, C. Niu, A. K. Dalai, *J. Environ. Sci.* **2019**, *83*, 46.

[18] a) O. Akeeb, L. Wang, W. Xie, R. Davis, M. Alkasrawi, S. Toan, *J. Environ. Manage.* **2022**, *313*, 115026; b) D. Jansen, M. Gazzani, G. Manzolini, E. Van Dijk, M. Carbo, *Int. J. Greenhouse Gas Control* **2015**, *40*, 167.

[19] a) D. Obi, S. Onyekuru, A. Orga, *Energy Sci. Eng.* **2025**, *13*, 1749; b) D. Thimsen, J. Wheeldon, D. Dillon, in *Oxy-Fuel Combustion for Power Generation and Carbon Dioxide (CO_2) Capture*, Elsevier, Amsterdam, **2011**, p. 17.

[20] X. Yan, M. Zhao, R. Yan, X. Wang, C. Dai, *J. Mol. Liq.* **2023**, *377*, 121521.

[21] M. Iddrisu, A. A. Umar, M. M. Hossain, *Arabian J. Sci. Eng.* **2025**, *50*, 9689.

[22] E. Pashayev, P. Georgopanos, *Macromol. Mater. Eng.* **2025**, *310*, 2400290.

[23] a) M. Wang, S. Zhou, S. Cao, Z. Wang, S. Liu, S. Wei, Y. Chen, X. Lu, *J. Mater. Chem. A* **2020**, *8*, 10519; b) M. Gallei, C. Rüttiger, *Chem—. Eur. J.* **2018**, *24*, 10006; c) L. Montero de Espinosa, W. Meesorn, D. Moatsou, C. Weder, *Chem. Rev.* **2017**, *117*, 12851; d) K. M. Herbert, S. Schrettl, S. J. Rowan, C. Weder, *Macromolecules* **2017**, *50*, 8845; e) P. Schattling, F. D. Jochum, P. Theato, *Polym. Chem.* **2014**, *5*, 25.

[24] C. De las Heras Alarcón, S. Pennadam, C. Alexander, *Chem. Soc. Rev.* **2005**, *34*, 276.

[25] F. Lang, J. Pang, X.-H. Bu, *eScience* **2024**, *4*, 100231.

[26] D. W. Löwik, E. Leunissen, M. van den Heuvel, M. Hansen, J. C. van Hest, *Chem. Soc. Rev.* **2010**, *39*, 3394.

[27] L. K. Rivera-Tarazona, Z. T. Campbell, T. H. Ware, *Soft Matter* **2021**, *17*, 785.

[28] S. Sankaran, S. Zhao, C. Muth, J. Paez, A. Del Campo, *Adv. Sci.* **2018**, *5*, 1800383.

[29] a) Q. Zhang, J. Zhang, S. Wan, W. Wang, L. Fu, *Adv. Funct. Mater.* **2018**, *28*, 1802500; b) S. Arnold, A. Gentile, Y. Li, Q. Wang, S. Marchionna, R. Ruffo, V. Presser, *J. Mater. Chem. A* **2022**, *10*, 10569.

[30] Z. Q. Cao, G. J. Wang, *Chem. Rec.* **2016**, *16*, 1398.

[31] H. Dong, L. Li, C. Li, *Chem. Sci.* **2023**, *14*, 8507.

[32] Y. Qiao, J. J. Bailey, Q. Huang, X. Ke, C. Wu, *Renewable Sustainable Energy Rev.* **2022**, *158*, 112079.
[33] Z. Yang, C. He, H. Sui, L. He, X. Li, *J. CO2 Util.* **2019**, *30*, 79.
[34] Y. Zeng, R. Zou, Y. Zhao, *Adv. Mater.* **2016**, *28*, 2855.
[35] S. Lin, P. Theato, *Macromol. Rapid Commun.* **2013**, *34*, 1118.
[36] R. Yuan, M. Zhang, H. Sun, *Polymers* **2023**, *15*, 1709.
[37] Z.-W. Liu, B.-H. Han, *Curr. Opin. Green Sustainable Chem.* **2019**, *16*, 20.
[38] B. Chen, H. Xie, L. Shen, Y. Xu, M. Zhang, M. Zhou, B. Li, R. Li, H. Lin, *Small* **2023**, *19*, 2207313.
[39] a) M.-y. Ding, Q.-y. Jiang, P.-c. Wu, H.-b. Jin, X.-l. Yang, S.-l. Lin, *Acta Polym. Sin.* **2025**, *56*, 690; b) A. Darabi, P. G. Jessop, M. F. Cunningham, *Chem. Soc. Rev.* **2016**, *45*, 4391.
[40] R. Lyndon, K. Konstas, R. A. Evans, D. J. Keddie, M. R. Hill, B. P. Ladewig, *Adv. Funct. Mater.* **2015**, *25*, 4405.
[41] S. Voskian, T. A. Hatton, *Energy Environ. Sci.* **2019**, *12*, 3530.
[42] M. M. Sadiq, H. Li, A. J. Hill, P. Falcaro, M. R. Hill, K. Suzuki, *Chem. Mater.* **2016**, *28*, 6219.
[43] M. M. Sadiq, K. Konstas, P. Falcaro, A. J. Hill, K. Suzuki, M. R. Hill, *Cell Rep. Phys. Sci.* **2020**, *1*,100070.
[44] A. B. Mabire, Q. Brouard, A. Pitto-Barry, R. J. Williams, H. Willcock, N. Kirby, E. Chapman, R. K. O'Reilly, *Polym. Chem.* **2016**, *7*, 5943.
[45] Y. Hu, Z. Liu, J. Xu, Y. Huang, Y. Song, *J. Am. Chem. Soc.* **2013**, *135*, 9287.
[46] D. Yuan, D. Zhao, H.-C. Zhou, *Inorg. Chem.* **2011**, *50*, 10528.
[47] H. Liu, Z. Liang, S. Wang, N. Ma, S. Chen, *J. Environ. Manage.* **2021**, *292*, 112722.
[48] H. Zhang, X. Meng, P. Li, *Prog. Chem.* **2008**, *20*, 657.
[49] P. Theato, B. S. Sumerlin, R. K. O'Reilly, T. H. Epps III, *Chem. Soc. Rev.* **2013**, *42*, 7055.
[50] S. Medeiros, A. Santos, H. Fessi, A. Elaissari, *Int. J. Pharm.* **2011**, *403*, 139.
[51] M. Karimi, M. Eslami, P. Sahandi-Zangabad, F. Mirab, N. Farajisafiloo, Z. Shafaei, D. Ghosh, M. Bozorgomid, F. Dashkhaneh, M. R. Hamblin, *Wiley Interdiscip. Rev. Nanomed. Nanobiotechnol.* **2016**, *8*, 696.
[52] L. Siegwardt, M. Gallei, *Adv. Funct. Mater.* **2023**, *33*, 2213099.
[53] A. G. Athanassiadis, Z. Ma, N. Moreno-Gomez, K. Melde, E. Choi, R. Goyal, P. Fischer, *Chem. Rev.* **2021**, *122*, 5165.
[54] W. Wu, R. Song, Z. Xu, Y. Jing, H. Dai, G. Fang, *Sens. Actuators, B* **2018**, *275*, 490.
[55] M. Zelzer, S. J. Todd, A. R. Hirst, T. O. McDonald, R. V. Ulijn, *Biomater. Sci.* **2013**, *1*, 11.
[56] Y. Lu, A. A. Aimetti, R. Langer, Z. Gu, *Nat. Rev. Mater.* **2016**, *2*, 16075.
[57] L. Li, H. Xing, J. Zhang, Y. Lu, *Acc. Chem. Res.* **2019**, *52*, 2415.
[58] a) P. Tan, Y. Jiang, X.-Q. Liu, L.-B. Sun, *ACS Energy Lett.* **2019**, *4*, 2656; b) A. B. Kanj, K. Müller, L. Heinke, *Macromol. Rapid Commun.* **2018**, *39*, 1700239.
[59] a) N. Yanai, T. Uemura, M. Inoue, R. Matsuda, T. Fukushima, M. Tsujimoto, S. Isoda, S. Kitagawa, *J. Am. Chem. Soc.* **2012**, *134*, 4501; b) H. Huang, H. Sato, T. Aida, *J. Am. Chem. Soc.* **2017**, *139*, 8784; c) H. Li, M. R. Martinez, Z. Perry, H. C. Zhou, P. Falcaro, C. Doblin, S. Lim, A. J. Hill, B. Halstead, M. R. Hill, *Chem—. Eur. J.* **2016**, *22*, 11176; d) R. Lyndon, K. Konstas, B. P. Ladewig, P. D. Southon, P. C. J. Kepert, M. R. Hill, *Angew. Chem.* **2013**, *125*, 3783.
[60] H. Li, M. R. Hill, C. Doblin, S. Lim, A. J. Hill, P. Falcaro, *Adv. Funct. Mater.* **2016**, *26*, 4815.
[61] Q.-R. Wu, P. Tan, C. Gu, R. Zhou, S.-C. Qi, X.-Q. Liu, Y. Jiang, L.-B. Sun, *Sci. China Mater.* **2021**, *64*, 383.
[62] A. Liu, G. Lu, X. Fan, C. H. Lau, *J. Mater. Chem. A* **2023**, *11*, 20559.
[63] H. Seo, J. Schretter, M. Massen-Hane, T. A. Hatton, *J. Am. Chem. Soc.* **2024**, *146*, 26777.
[64] a) G. Kumari, K. Jayaramulu, T. K. Maji, C. Narayana, *J. Phys. Chem. A* **2013**, *117*, 11006; b) Y. Liu, J.-H. Her, A. Dailly, A. J. Ramirez-Cuesta, D. A. Neumann, C. M. Brown, *J. Am. Chem. Soc.* **2008**, *130*, 11813; c) H. Wu, C. G. Thibault, H. Wang, K. A. Cychosz, M. Thommes, J. Li, *Microporous Mesoporous Mater.* **2016**, *219*, 186.
[65] M. Yue, K. Imai, Y. Miura, Y. Hoshino, *Polym. J.* **2017**, *49*, 601.
[66] G. Hu, Z. Xiao, K. Smith, S. Kentish, G. Stevens, L. A. Connal, *Chem. Eng. J.* **2018**, *332*, 556.
[67] a) P. D. Werz, J. Kainz, B. Rieger, *Macromolecules* **2015**, *48*, 6433; b) A. Sanna, M. Dri, M. Maroto-Valer, *Fuel* **2013**, *114*, 153.
[68] a) J. Beiron, F. Normann, L. Kristoferson, L. Stromberg, S. O. Gardarsdottir, F. Johnsson, *Ind. Eng. Chem. Res.* **2019**, *58*, 14275; b) H. Seo, M. P. Nitzsche, T. A. Hatton, *Acc. Chem. Res.* **2023**, *56*, 3153.
[69] Z. Hu, J. Lin, N. Ogiwara, A. Rodriguez, Y. Peng, Y. Wang, S. Horike, D. Zhao, *CrystEngComm* **2016**, *18*, 2803.
[70] M. R. Lohe, K. Gedrich, T. Freudenberg, E. Kockrick, T. Dellmann, S. Kaskel, *Chem. Commun.* **2011**, *47*, 3075.
[71] K. Dutta, S. De, *J. Mater. Chem. A* **2017**, *5*, 22095.
[72] M. M. Sadiq, M. Rubio-Martinez, F. Zadehahmadi, K. Suzuki, M. R. Hill, *Ind. Eng. Chem. Res.* **2018**, *57*, 6040.
[73] H. Li, M. M. Sadiq, K. Suzuki, R. Ricco, C. Doblin, A. J. Hill, S. Lim, P. Falcaro, M. R. Hill, *Adv. Mater. (Deerfield Beach, Fla.)* **2016**, *28*, 1839.
[74] W. Li, J. Wu, S. S. Lee, J. D. Fortner, *Chem. Eng. J.* **2017**, *313*, 1160.
[75] a) A. L. Black, J. M. Lenhardt, S. L. Craig, *J. Mater. Chem.* **2011**, *21*, 1655; b) A. C. Overholts, W. G. Razo, M. J. Robb, *Nat. Chem.* **2023**, *15*, 332; c) I. Beurroies, M. Boulhout, P. L. Llewellyn, B. Kuchta, G. Féray, C. Serre, R. Denoyel, *Angew. Chem., Int. Ed.* **2010**, *49*, 7526.
[76] a) H. Guo, W. Zhang, N. Lu, Z. Zhuo, X. C. Zeng, X. Wu, J. Yang, *J. Phys. Chem. C* **2015**, *119*, 6912; b) Y. Tao, Q. Xue, Z. Liu, T. Zhang, X. Li, T. Wu, Y. Jin, L. Zhu, *Sci. Adv. Mater.* **2015**, *7*, 239; c) T. Winter, M. Bitsch, F. Müller, S. Voskian, T. A. Hatton, K. Jacobs, V. Presser, M. Gallei, *ACS Appl. Polym. Mater* **2021**, *3*, 4651.
[77] G. Iijima, J. Naruse, H. Shingai, K. Usami, T. Kajino, H. Yoto, Y. Morimoto, R. Nakajima, T. Inomata, H. Masuda, *Energy Fuels* **2023**, *37*, 2164.
[78] A. M. Zito, D. Bím, S. Vargas, A. N. Alexandrova, J. Y. Yang, *ACS Sustainable Chem. Eng.* **2022**, *10*, 11387.
[79] Y. Guo, M. Massen-Hane, G. Endy, T. A. Hatton, *Adv. Mater.* **2024**, *36*, 2407567.
[80] J. Liu, M. Yang, X. Zhou, Z. Meng, *J. Am. Chem. Soc.* **2024**, *146*, 33093.
[81] H. Li, M. E. Zick, T. Trisukhon, M. Signorile, X. Liu, H. Eastmond, S. Sharma, T. L. Spreng, J. Taylor, J. W. Gittins, *Nature* **2024**, *630*, 654.
[82] Q. Yan, Y. Zhao, *Chem. Commun.* **2014**, *50*, 11631.
[83] a) C. Zeng, J. Dai, T. Yang, Z. Wang, Y. Gao, J. Xia, Y. Chen, M. Sun, *Dyes Pigm.* **2024**, *222*, 111906; b) Y. Zhang, S. Zhang, C. Liang, J. Shi, L. Ji, *Adv. Mater.* **2023**, *35*, 2302732.
[84] D. Zhang, X. Lu, Y. Li, G. Wang, Y. Chen, J. Jiang, *Colloids Surf. A* **2018**, *543*, 155.
[85] G. Puxty, R. Rowland, A. Allport, Q. Yang, M. Bown, R. Burns, M. Maeder, M. Attalla, *Environ. Sci. Technol.* **2009**, *43*, 6427.
[86] a) S. Jin, M. Wu, R. G. Gordon, M. J. Aziz, D. G. Kwabi, *Energy Environ. Sci.* **2020**, *13*, 3706; b) H. Xie, Y. Wu, T. Liu, F. Wang, B. Chen, B. Liang, *Appl. Energy* **2020**, *259*, 114119.
[87] a) D. Bilger, F. Ali, E. D. Patamia, C. Payne, T. L. Andrew, D. G. Kwabi, *Electrochem. Soc. Meet. Abstr.* **2024**, *245*, 1532; b) Y. Jing, K. Amini, D. Xi, S. Jin, A. M. Alfaraidi, E. F. Kerr, R. G. Gordon, M. J. Aziz, *ACS Energy Lett.* **2024**, *9*, 3526; c) F. Ali, D. Bilger, E. D. Patamia, T. L. Andrew, D. G. Kwabi, *J. Electrochem. Soc.* **2024**, *171*, 053505.
[88] S. Jin, M. Wu, Y. Jing, R. G. Gordon, M. J. Aziz, *Nat. Commun.* **2022**, *13*, 2140.
[89] S. Pang, S. Jin, F. Yang, M. Alberts, L. Li, D. Xi, R. G. Gordon, P. Wang, M. J. Aziz, Y. Ji, *Nat. Energy* **2023**, *8*, 1126.
[90] a) Q. Huang, Z. Zhan, R. Sun, J. Mu, B. Tan, C. Wu, *Angew. Chem.* **2023**, *135*, 202305500; b) F. Castiglioni, W. Danowski, J. Perego, F.

K.-C. Leung, P. Sozzani, S. Bracco, S. J. Wezenberg, A. Comotti, B. L. Feringa, *Nat. Chem.* **2020**, *12*, 595.
[91] W. Luo, W. Lu, Q. Xiang, L. Zhan, X. Yang, H. Jiang, C. Xu, H. He, *Chem. Eng. J.* **2024**, *489*, 151144.
[92] J. Park, D. Yuan, K. T. Pham, J.-R. Li, A. Yakovenko, H.-C. Zhou, *J. Am. Chem. Soc.* **2012**, *134*, 99.
[93] J. Wu, B. Pourdeyhimi, A. L. Yarin, *Macromol. Rapid Commun.* **2024**, 2400861.
[94] a) W. Yang, H. Liu, *Acta Chim. Sin.* **2015**, *73*, 623; b) J. Kainz, P. D. L. Werz, C. Troll, B. Rieger, *RSC Adv.* **2015**, *5*, 9556.
[95] K. Wang, L. An, G. Lu, J. Zhang, Z. Wang, M. Si, G. Liu, Y. Zeng, *Polymer* **2023**, *280*, 126039.
[96] K. Wang, X. Liu, Z. Li, F. Zhao, G. Liu, Y. Zeng, *Macromolecules* **2025**, *58*, 5208.
[97] a) B. Li, B. Chen, *Sci. China: Chem.* **2016**, *59*, 965; b) K. Roztocki, M. Rauche, V. Bon, S. Kaskel, E. Brunner, D. Matoga, *ACS Appl. Mater. Interfaces* **2021**, *13*, 28503.
[98] a) A. J. Allen, L. Espinal, W. Wong-Ng, W. Queen, C. Brown, S. R. Kline, K. L. Kauffman, J. T. Culp, C. Matranga, *J. Alloys Compd.* **2015**, *647*, 24; b) A. G. Kontos, G. E. Romanos, C. M. Veziri, A. Gotzias, M. K. Arfanis, E. Kouvelos, V. Likodimos, G. N. Karanikolos, P. Falaras, *Appl. Surf. Sci.* **2020**, *529*, 147058; c) D.-D. Zhou, C.-T. He, P.-Q. Liao, W. Xue, W.-X. Zhang, H.-L. Zhou, J.-P. Zhang, X.-M. Chen, *Chem. Commun.* **2013**, *49*, 11728.
[99] J. Liu, B. Li, V. Martins, Y. Huang, Y. Song, *J. Phys. Chem. C* **2024**, *128*, 8007.
[100] K. Wang, M. Si, X. Liu, Z. Wang, G. Liu, Y. Zeng, *Polym. Chem.* **2024**, *15*, 3795.
[101] M. Singh, A. Karmakar, N. Seal, P. P. Mondal, S. Kundu, S. Neogi, *ACS Appl. Mater. Interfaces* **2023**, *15*, 24504.
[102] S. Zhou, M. Wang, J. Wang, H. Xin, S. Liu, Z. Wang, S. Wei, X. Lu, *J. Mater. Chem. A* **2020**, *8*, 9970.
[103] K. Wang, J. Zhang, M. Si, Z. Wang, L. An, G. Liu, Y. Zeng, *Macromolecules* **2023**, *56*, 9127.

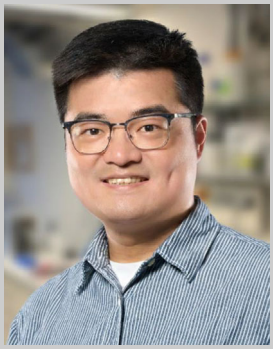

Jian Zhou is currently a postdoctoral researcher at Saarland University under the host of Prof. Markus Gallei. He obtained his Ph.D. from University of Science and Technology of China in 2022. His research interests mainly focus on the application of intelligent polymers for energy and sustainability, with a particular emphasis on electrochemical approaches.

Marc Deissenroth-Uhrig is professor at the University of Applied Scienes of Saarland (htw saar) and researcher at the Institut for Future Energy Systems (IZES). He received his PhD in physics from the University of Heidelberg in the field of high energy physics in 2010. After gaining experiences in the utility sector as consultant at SAP Deutschland AG & Co. KG from 2010 to 2013, he was reseacher at the German Aerospace Center from 2013 to 2020. He has deep knowledge in the field of energy system transformation and modeling and leads interdisciplinary projects with experts from social sciences, economy and technology.

Markus Gallei is the Chair of Polymer Chemistry at Saarland University and Director of Saarene Saarland Center of Energy Materials and Sustainability. He worked as a Junior Researcher Group Leader at TU Darmstadt (Germany, 2011–2018). For his Ph.D. research, he worked in the field of functional metallopolymers at the German Institute for Polymers (DKI) in Darmstadt, receiving his Ph.D. in 2010. In 2011, he was a postdoc at the Helmholtz Centre Geesthacht, working on stimuli-responsive polymer membranes. In 2017 and 2018, he was visiting scientist at the MIT (Cambridge, USA) in the group of T. Alan Hatton. He received the Reimund-Stadler-Prize of the GDCh in 2018. His research focuses on the design of intelligent polymer architectures for optical sensing, structural colors, sorption of molecules and smart switchable membranes.